175900-12-F

AFOSR-TR- 88-0095

Final Report

OPTICAL SWITCHING AND CONTROL TECHNIQUES USING NONLINEAR OPTICAL WAVE MIXING

AD-A190 467

L.M. PETERSON
Optical Science Laboratory
Advanced Concepts Division

DECEMBER 1987

Defense Advanced Research Projects Agency
1400 Wilson Blvd.
Arlington, VA 22209

ERIM P.O. Box 8618
Ann Arbor, MI 48107-8618

UNCLASSIFIED

SECURITY CLASSIFICATION OF THIS PAGE

REPORT DOCUMENTATION PAGE

1a. REPORT SECURITY CLASSIFICATION UNCLASSIFIED	1b. RESTRICTIVE MARKINGS AD-190467
2a. SECURITY CLASSIFICATION AUTHORITY	3. DISTRIBUTION/AVAILABILITY OF REPORT Unlimited
2b. DECLASSIFICATION/DOWNGRADING SCHEDULE	
4. PERFORMING ORGANIZATION REPORT NUMBER(S) 175900-12-F	5. MONITORING ORGANIZATION REPORT NUMBER(S) AFOSR-TR- 88-0095
6a. NAME OF PERFORMING ORGANIZATION Environmental Research Institute of Michigan 6b. OFFICE SYMBOL (if applicable)	7a. NAME OF MONITORING ORGANIZATION Air Force Office of Scientific Research
6c. ADDRESS (City, State, and ZIP Code) P.O. Box 8618 Ann Arbor, MI 48107	7b. ADDRESS (City, State, and ZIP Code) Building 410 Attn: Dr. Lee Giles Bolling AFB, D.C. 20332
8a. NAME OF FUNDING/SPONSORING AFOSR/NE BLDG 410 BOLLING AFB, DC 20332-6448 8b. OFFICE SYMBOL	9. PROCUREMENT INSTRUMENT IDENTIFICATION NUMBER F49620-84-C-0067 10. SOURCE OF FUNDING NUMBERS PROGRAM ELEMENT NO. 61102F; PROJECT NO. DARPA; TASK NO 4952; WORK UNIT ACCESSION NO

11. TITLE (Include Security Classification)
Optical Switching and Control Techniques Using Nonlinear Optical Wave Mixing (U)

12. PERSONAL AUTHOR(S)
Lauren M. Peterson

13a. TYPE OF REPORT	13b. TIME COVERED	14. DATE OF REPORT (Year, Month, Day)	15. PAGE COUNT
Final	FROM 9/15/85 6/15/87	December 1987	

16. SUPPLEMENTARY NOTATION
ARPA Order 4952 Contract Number F49620-84-0067
Program Code 3D10 Contract Period: 6/15/84-6/15/87

17. COSATI CODES		
FIELD	GROUP	SUB-GROUP

18. SUBJECT TERMS (Continue on reverse if necessary and identify by block number)
Optical Computing; Nonlinear Optics; Thermal Effects; Optical Switching; Stimulated Scattering; Forced Rayleigh Scattering

19. ABSTRACT (Continue on reverse if necessary and identify by block number)

Optical nonlinearities of thermal origin are considered by many to be slow and therefore of limited practical use. We show experimentally that thermo-optically induced (1) beam guides and (2) phase grating structures can be used to efficiently switch an optical beam by redirecting its energy in times of 20 and 2 nsec, respectively.

The beam guiding was achieved by passing a focused, TEM_{00} laser pulse through an absorbing liquid to which an absorbing dye had been added. Heating of the liquid in the focal region by the Gaussian profile beam changed the refractive index to produce a long cylindrical volume analogous to a graded-index (GRIN) optical fiber. Radiation from a second laser beam not absorbed by the liquid could be coupled into the graded index real-time "fiber" and redirected by it with an efficiency as high as 90 percent. The switch-on time was measured to be 20 nsec and persisted without intervention for about 1

20. DISTRIBUTION/AVAILABILITY OF ABSTRACT ☒ UNCLASSIFIED/UNLIMITED ☐ SAME AS RPT ☐ DTIC USERS	21. ABSTRACT SECURITY CLASSIFICATION UNCLASSIFIED
22a. NAME OF RESPONSIBLE INDIVIDUAL Giles	22b. TELEPHONE (Include Area Code) (202) 767-4933 22c. OFFICE SYMBOL NE

DD FORM 1473, 84 MAR

UNCLASSIFIED

SECURITY CLASSIFICATION OF THIS PAGE

#19 Continued

millisecond (i.e. optical memory). The rise and decay times are in good agreement with calculations using a simple thermal model which describes the process.

The thermo-optically induced phase grating was generated by interfering two beams of laser radiation in an absorbing liquid. Heating of the liquid along the interference pattern produced a sinusoidally varying refractive index pattern or phase grating. This real-time optically generated grating was used to switch (redirect by diffraction) a probing laser beam. For a small crossing angle of 7°, a switching time of 2 nsec was measured and was in good agreement with the thermal model, as was the measured diffraction efficiency of 15 percent. The thermal model which accurately predicted the results of our experiments predicts that by varying the crossing angle from near-zero to near 180°, switch-on times of from 0.1 to 10 nsec are possible and persistence times of from 1 nsec to more than 1 msec are possible. This temporal flexibility translates to high repetition rates and optical memory, respectively.

Considering the two interfering beams producing the phase grating to be two inputs, and the diffracted probe beam to be the output, a logical AND gate was demonstrated experimentally and had a very high contrast ratio. OR, XOR, NAND and NOR as well limiting and inversion should be achievable using analogous geometries but time limitations did not allow these to be demonstrated experimentally. Optical amplification was investigated on a limited level of effort early in the program and was demonstrated with moderate gain. Extension of this work with a broadened scope is warranted.

The phase grating structure appears to be particularly well suited for extension to a 2-D array for taking advantage of the parallelism offered by optics. However, since 10μJ pulses were necessary to observe efficient thermo-optic guides and gratings, this scales to about 1Kw of average optical power (100w of heat dissipation) to achieve a modest 10 x 10 array at a switching rate of 10^6 sec^{-1}. Clearly, improvements in switching energy are necessary before parallelism and speed may be effectively implemented.

Though the emphasis in this program was on basic component development, such componentry has a potentially wide applicability to optical computer/processor systems and optical control devices. Applied system oriented research in these areas is a logical aspect of future development activity for this technology.

PREFACE

The work reported here was performed in the Optical Sciences Laboratory, which is part of the Advanced Concepts Division at ERIM. The work was supported by the Defense Advanced Research Projects Agency under the direction of Dr. John A. Neff and was monitored by the Air Force Office of Scientific Research under Contract No. F49620-84-C-0067. Col. Robert Carter was program manager for the AFOSR during the initial phases of this program and was succeeded by Dr. Lee Giles later on in the program.

This final technical report covers work performed from 15 June 1984 to 15 June 1987 with emphasis placed upon the final year of the program. The principle investigator at ERIM was Dr. Lauren M. Peterson, and Patrick Hamilton was a major contributor to the experimental work.

TABLE OF CONTENTS

LIST OF FIGURES

LIST OF TABLES

1
INTRODUCTION

1.1 BACKGROUND

The inherent parallelism of optical processing systems enables one to process data at a rate unmatched by current electronic digital counterparts. Coherent optical processors for example, have been used to process data gathered by synthetic aperture radars since the early sixties [1,2]. Despite the fact that the technology is two decades old, it still holds a distinct advantage over electronic digital processing systems in throughput within its computing channel.

The precision of an optical analog processor is restricted by the dynamic range of the output detector or the input spatial light modulator while the accuracy of the system is limited by the achievable optical quality of the optical components such as lenses and mirrors. To achieve programability and high precision, it is logical to mate optical concepts with digital concepts and develop a numerical optical computer. Such a task however, makes sense only if an optical computer can offer specific and substantial advantages over the well established electronic implementations [3-5].

Optics offers an alternate means of increasing the system speed and parallelism without resorting to superconductivity under cryogenic conditions. Since light beams can traverse each other without interference, cross talk is minimized and three-dimensional (as opposed to planar) circuit structure can be implemented. Thus, at least potentially, a higher packing density, and in turn a higher degree of parallelism, can be realized with an optical numerial computer.

The logical progression from an all-electronic computer would first include an electronic-optical hybrid device. Respective advantages

could be taken of both the electronic and the optical properties although tranducers would be necessary to convert from the electronic domain to the optical and back again. Significant improvements in speed, complexity and size could be further realized by replacing the electronic functions with optical equivalents thereby eliminating the need for transducers within the device and enabling an all-optical device.

All-electronic devices rely upon electrical signals to control electrical currents or voltages. Electronic-optical devices rely upon electrical signals to control optical beams of radiation (i.e., electro- and acousto-optic components) or vise-versa (i.e., detectors). An all-optical device must rely upon optical signals to control optical beams [6]. In linear optics, one beam of radiation cannot interact with another beam of radiation. This provides the means for data networking with three-space multiplexing in the absence of cross talk, thus the attractive prospect of highly parallel processing. However, if the electromagnetic field of one or both beams of radiation is large enough and the beams cross in a material medium, then the beams can interact and influence each other. The high field condition drives the medium into a region of nonlinearity. The phenomenon of light interacting with light via a material medium is classified as nonlinear optics and is the basis of the proposed effort. The overlapping of radiation fields in a nonlinear medium can lead to methods of optical control such as optical switching, limiting or clipping, amplification and beam steering.

The application of optical control concepts considered in this program is potentially quite extensive. The recommendations noted above are of course component oriented. It is also recommended that system oriented applications be pursued as a logical extension to the component development. Examples include switches, nonlinear operators, amplification and beam positioning for neural network optical computing, agile beam steering for sensor systems, and more generally, use in a

wide range of analog or digital optical processing systems and in optical control devices.

1.2 PROGRAM SUMMARY

The research effort described in this report was directed toward exploring the control of one light beam by the action of another light beam. The motivation for the effort was provided by the properties of stimulated thermal Rayleigh scattering (STRS) [9] which showed potential for being able to provide the desired all-optical control functions of optical switching, clipping and amplification. Although STRS entails self-switching, clipping (thresholding) and amplification (gain), it is not in a form which may readily be used for optical control. The research plan was to study STRS in the context of beam control not only in its usual on-axis geometry using simple focusing lenses and a single input pump beam, but rather explore other geometries including off-axis configurations, cylindrical optics and multiple beams in order to explore, characterize and exploit the interaction process [7].

Since the mechanism of STRS is thermal in origin and entails the creation of thermal phase gratings in absorbing media through optical mixing of signal and pump radiation, the generation of thermal phase gratings in various geometries was examined. The interference of two coherent electromagnetic waves of the same frequency with an angle θ between their propagation vectors leads to a standing wave as shown in Figure 1.1 whose spatial periodicity is

$$\Lambda = \frac{\lambda}{2 \sin (\theta/2)}$$

where λ is the wavelength of the radiation in the medium and θ is the crossing angle of the radiation in the medium. STRS is observed with $\theta = 180°$ where one beam is the laser beam itself and the second beam is

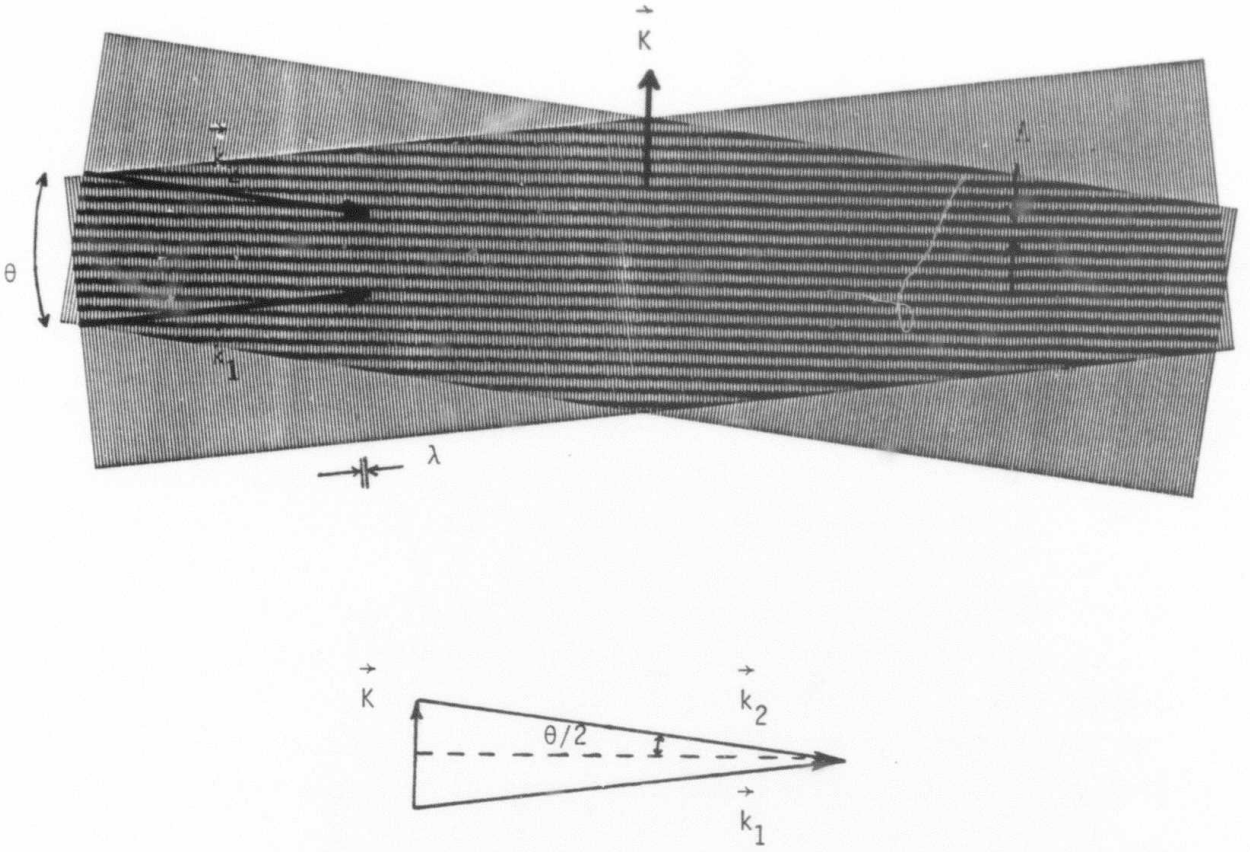

Fig. 1.1 Interference of two coherent beams of radiation crossing at an an angle of θ. k_1 and k_2 are radiation wave vectors and k is a wave vector for the resulting interference pattern.

180° spontaneous Rayleigh scattering [9]. A thermally generated phase grating of spacing $\Lambda = \lambda/2$ is produced by the interference pattern and leads to gain of the back scattered light and to the stimulated scattering. A variation on this is to use the same 180° geometry and inject a signal beam rather than relying upon weak spontaneously Rayleigh scattered light and is reported in the first semi-annual report [10]. This may be referred to as Forced Rayleigh scattering (FRS) [11,12]. The advantage of FRS is the control of the signal power, polarization and direction by the experimenter which is not available in STRS. An advantage of STRS is the continuum of frequencies present in the slight broadening encountered in the Rayleigh scattering process. An acousto-optic modulator was used to emulate that broadening for FRS by providing an up- or down-shift of 50 MHz on the signal beam [10]. STRS theory predicts that the gain for the up-shifted signal should increase compared to the gain for unshifted signal radiation and the gain for the down-shifted signal should decrease. Experimentally, we observed no change in the gain whether up- or down-shifting [10]. This is not surprising, however, considering the moderate spectral purity of the multi-longitudinal mode laser used in the experiments and its short coherence length of only a fraction of a millimeter.

In the performance of these experiments, a HeNe laser was used to probe the interaction between the dye laser light pulses and the absorbing liquids. A new and interesting phenomena was observed whereby the probe propagation was modified by the passage of a single laser pulse through the absorbing medium. This phenomena has been attributed to heating of the liquid in the long cylindrical focal volume, and subsequent changing of the density and refractive index to create a graded index beam guide quite analogous to a fiber. The HeNe laser radiation is coupled into the real-time "fiber" and is guided by it for times on the order of a millisec corresponding to the thermal diffusion of the temperature perturbation. Switch-on times were on the order of nanoseconds using microjoule pulses and efficiencies were good. A

maximum efficiency of 96 percent was measured. These experiments are described in Section 2.

The laser source for these experiments was a Molectron SP-10 nitrogen laser pumped dye laser whose spectral linewidth was 0.7 nm (30 cm^{-1}) and contained numerous longitudinal modes. The need for spectral purity led to the purchase of an LSI Model 337130 grazing incidence dye laser [13] whereby the spectral linewidth was decreased by roughly a factor of ten and the coherence length was increased to 3 mm. Using this laser, experiments were conducted at small angles of intersection, θ, and therefore fringe spacing of $\Lambda \gg \lambda$. Section 3 describes these experiments and the efficient optical switching which was obtained using microjoule laser pulses and nanosecond switching times.

The optical switching which was demonstrated was also operated as an all-optical 3-port logical AND-gate. Two optical beams were the input and the output was in the form of a third beam. Output was only exhibited when both inputs were "on" and the contrast ratio was good. Other logical gates including EOR, XOR, NOR, NAND and NOT should be possible using similar geometries and are discussed in Section 3. Also discussed are the implementation of optical limiting, inversion and amplification using the phase grating structure, although they were not demonstrated experimentally.

Section 4 provides a discussion of the results and conclusions of the program. Section 5 provides recommendations for further work in this area.

2
REAL-TIME BEAM GUIDING IN ABSORBING LIQUIDS

Radiation passing through a nonlinear optical medium can lead to a change in the refractive index of that medium. If the radiation is in the form of a focused Gaussian laser beam, the focal region will have a refractive index profile which is bell-shaped in the transverse direction. For a large f-number focused beam, the focal region is a long cylinder with a transverse graded-index (GRIN) profile quite analogous to a graded index waveguide or fiber. We have used this real-time refractive index waveguide due to one beam of pulsed laser radiation to rapidly redirect or switch a second beam of laser radiation [8].

The material media in which we have observed real-time beam guiding are liquids to which dyes have been added to make the liquid optically dense. The refractive index changes have been induced by absorption of the radiation followed by rapid ($\sim 10^{-10}$ sec [14] thermalization of the energy. The change in temperature of the liquid leads to the change in its refractive index (presumably due to local changes in density).

2.1 EXPERIMENTAL

Figure 2.1 shows the experimented arrangement used for observing real-time beam guiding. The pulsed radiation source is a Molectron SP-10 nitrogen laser which pumps a Laser Sciences Inc. grazing incidence dye laser of Littman design [15]. Using Coumarin 500 dye, the output was a maximum 25 μJ at 510 nm. The laser pulse duration was approximately 5 nsec and the peak power was 5 Kw. The dye laser output was beam expanded to 5 mm and focused using lens L1, an f/2.7, 152 mm Baltar lens (effective f-number of 30). The continuous probing radiation was provided by a Spectra Physics Model 125 HeNe laser beam expanded to 5 mm and also focussed by lens L1. In order to eliminate

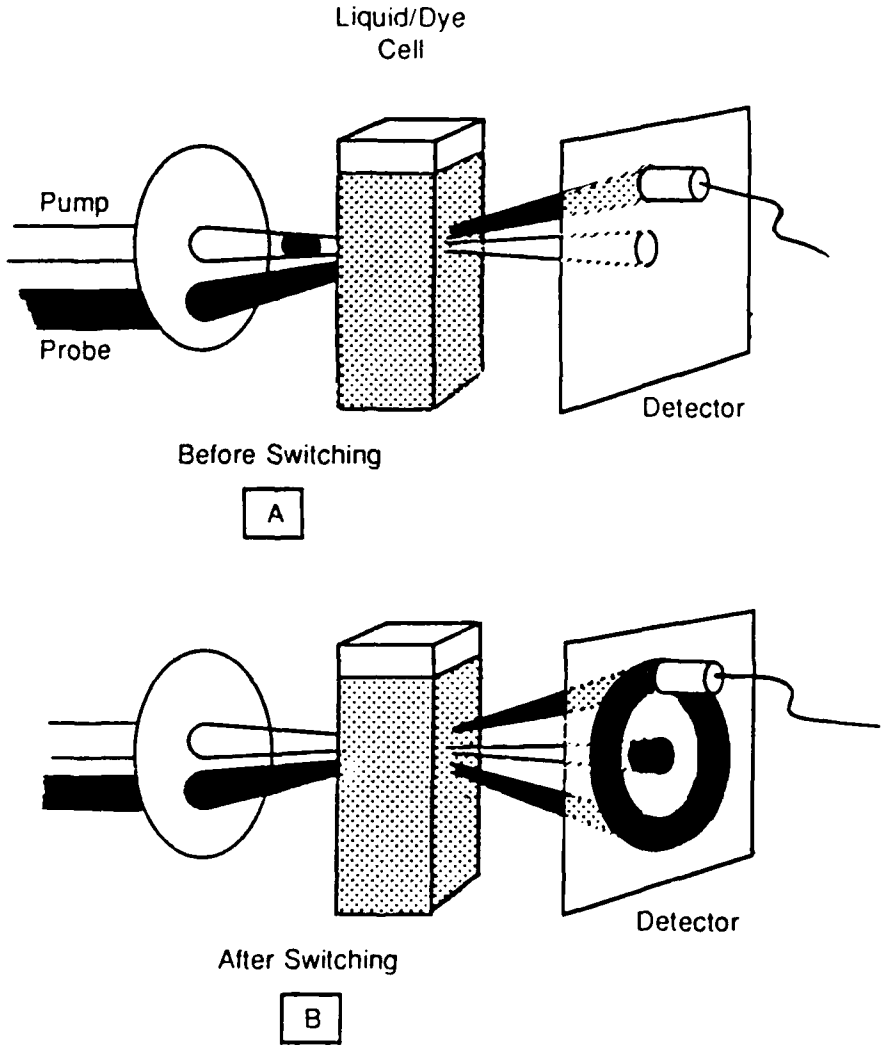

Fig. 2.1 Experimental arrangement for observing the thermo-optical beam guide and switch.

any thermal interactions due to the probe radiation, the HeNe was attenuated to about 1 mW and chopped to provide low duty cycle square pulses in synchronization with the 30 pps repetition rate of the pulsed laser. The pulsed dye laser and HeNe probe laser beams were both collimated and carefully aligned to be parallel to each other such that they would cross in their focal regions. The nearly cylindrical focal region was measured to be 30 μm in diameter and had a length of about 1.2 mm.

The liquid sample was contained in a 1x1x10 cm glass cell. Carbon disulfide, CS_2, carbon tetrachloride, CCl_4, methanol, CH_3OH, ethanol, C_2H_5OH, water, H_2O, and acetone, $(CH_3)_2CO$, were used as host liquids to which the red dyes iodine, I_2, cobalt nitrate, $Co(NO_3)_2$, eosine, $C_{20}H_8Br_4O_5$ (a fluorescent dye), rhodamine 590 (a laser dye) and cresyl violet perchlorate (a laser dye) were added (see Table I). Red dyes were chosen to be highly absorbing at the pulse wavelength yet of low absorption at the probe wavelength. Concentrations were adjusted to provide attenuation of the green pulses in the range of 0.1 to 10 cm^{-1} (see Appendix E). Some of the material parameters for these liquids are provided in Table II. After passing through the sample, the transmitted radiation was filtered using a 632.8 nm spectral interference filter. It was then detected by an RCA 8645 or 1P28 photomultiplier tube or by an HP4203 Si PIN detector, all having response times on the order of 1 nsec.

As the dye laser pulse passes through the absorbing sample, some of the radiation is absorbed by the dye molecules. This energy is rapidly thermalized ($\sim 10^{-10}$ sec [14]) and appears as a deviation from equilibrium. Since the laser intensity profile is Gaussian distributed in the transverse direction, the transverse temperature profile and likewise the refractive index profile will have bell-shaped distributions. In the longitudinal direction, since the laser beam is attenuated as it propagates the change in temperature and therefore the

Table I

Solvents and Dyes Used in Beam Guiding Experiments

	CS_2	$C Cl_4$	CH_3OH	H_2O	Acetone
I_2	96	70	45		
$Co(NO_3)_2$			30	7	45
Eosine			20		
R590			10		
CVP			35		

The numbers indicate the maximum efficiency (in percent) for beam guiding using 10 μJ laser pulses at 510 nm.

Table II. Material parameters for selected liquids [9(b)]

Liquid	n	ρ (gm/cm^3)	C_p (erg/g°K)	β_v ($°K^{-1}$)	κ_T[a] (mw $cm^{-1}K^{-1}$)	dn/dT ($°K^{-1}$) measured[b]	dn/dT ($°K^{-1}$) calculated[c]	t^d_{relax} (nsec)	V_{sound} (cm/sec)	Γ_B[e] (MHz)	Γ_R[f] (MHz)
Carbon tetrachloride	1.46	1.591	0.84×10^{7}	1.18×10^{-3}	1.07	--	6.73×10^{-4}	0.13	0.95×10^{5}	630	18
Acetone	1.36	0.791	2.1	1.32	1.6	--	6.03	--	1.19	270	21
Methyl alcohol	1.33	0.794	2.5	1.18	2.0	--	4.40	0.013	1.21	300	12
Carbon disulfide	1.63	1.263	0.95	1.14	--	--	10.05	2.83	1.17	65	37
Benzene	1.50	0.880	1.7	1.18	1.32	6×10^{-4}	7.48	0.27	1.17	350	27
Ethyl ether	1.35	0.715	2.3	1.51	1.37	6	6.59	--	1.03	290	16
Water	1.33	1.343	4.2	0.20	6.04	-	0.77	--	1.46	380	26
Ethyl alcohol	1.36	0.800	2.4	1.12	1.7	4	4.58	1.7	1.21	--	--

a) Thermal conductivity [16] p. 4-85.

b) Thermo-optic coefficient [16] p. 6-90

c) From equation (A.6) for λ = 486 nm; β_v from [16] p. 4-75.

d) Thermal relaxation time, from Hertzfeld and Litovitz [14] Table 95-1.

e) Brillouin linewidth [17]; $\Gamma_B = \eta k^2/\rho$; η is viscosity, $k = |k_L - k_S| = 2\pi/\Lambda$; these values are 1.2 times greater than those presented by Shen [18], Table 11.1.

f) Rayleigh linewidth $\Gamma_R = 2\kappa_T k^2/\rho C_p$; λ = 694nm, 180° scattering.

change in refractive index will decrease slowly with distance. Over the fraction of a millimeter focal volume the variation should be only a few percent and can be ignored.

2.2 RESULTS

When the pulse of green radiation and the red probe were focused into air or into a clear liquid sample, the two beams did not interact and simply crossed in the focal regions. A screen placed behind the sample cell displayed the two beams of radiation as shown in Figure 2.2(a). When the two beams of radiation were focused into a liquid sample containing sufficient absorber, the red probe radiation was distributed into an annulus surrounding the transmitted green beam as shown in Figure 2.2(b). Presumably the intense pulse of radiation induces a cylindrically symmetric focal region whose refractive index differs from the surrounding medium. The small angle between the propagation of the green pulse and that of the red probe allows the latter to be coupled into and guided by the real-time refractive index perturbation. Multiple reflections within the cylindrical guide lead to a redistribution of the red radiation into two dimensions while maintaining the initial angle of entrance just as one encounters for an optical fiber. This results in a cone of red light emerging from the focal region and is recorded as a ring of red light surrounding the cylindrical axis marked by the presence of the green radiation as shown in Figure 2.2(b).

Once the green dye laser pulse, whose duration is only a few nanoseconds, has passed through the sample and thermally excites the refractive index guide, that guide persists until thermal diffusion effects cause the medium to return to thermal equilibrium. Due to the cylindrical symmetry of the thermal perturbation, the diffusion process is radially outward leading to a bell-shaped temperature (and refractive index) profile whose width increases and whose magnitude on-axis

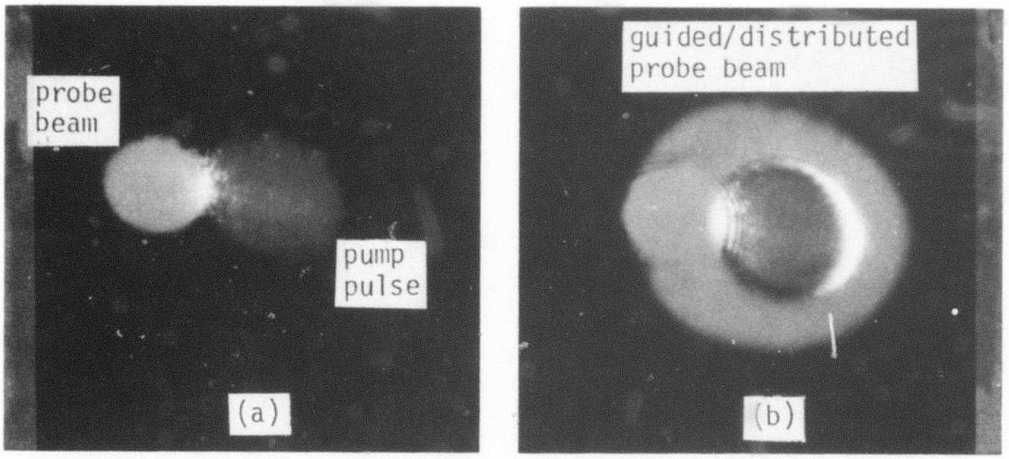

Fig. 2.2 Output beam patterns. Absence of absorber in (a) results in no beam guiding. Absorbing liquid in (b) results in beam guiding.

decreases. Computations show that for a 10 μJ laser pulse focused to a waist radius of 15 μm, a distance of 3 mm into carbon disulfide containing a dye whose absorption is 3 cm^{-1}, an average temperature increase of 0.64^{o}K and a refractive index change of 4.3×10^{-4} is predicted (see Section 3.3).

2.2.1 Temporal Response

The experiment depicted in Figure 2.1 was used to determine the temporal properties of the beam guide interaction. A fast detector (Si PIN or PM tube) was used to monitor the intensity of the HeNe probe radiation which passed through the experimental sample cell as shown. Figure 2.3 shows the signal recorded from that detector, with HeNe radiation intensity represented in the vertical direction. The chopped square pulse of HeNe radiation was 10 msec in duration and the rise of that pulse provided the trigger for the traces. Approximately 50 μsec after turn-on of the HeNe beam, the pulsed dye laser operating at a wavelength of 510 nm was fired. The top trace in Figure 2.3 represents the HeNe radiation signal in the presence of a low energy (about 1 μJ) green pulse. The other traces correspond to progressively higher energy green pulses with increments of 1 μJ, up to a maximum of 10 μJ for the bottom trace. The presence of the green pulse is obvious since the amount of HeNe radiation drops abruptly. It should be emphasized that the time scale for the scope trace is 100 μsec per division and that the green pulse duration is only 5 nsec. It should also be noted that the high frequency modulation at 160 μsec is simply an artifact due to a defect in the mechanical chopper used in the HeNe laser beam.

Moving the detector to the diametrically opposite position on the ring of light in Figure 2.1B showed that the risetime for generation of the beam guide was 20 nsec as can be seen in the top trace in Figure 2.4. This risetime also corresponds to the rapid fall-time in Figure 2.3. Although RFI noise due to the laser thyratron switch prevented an

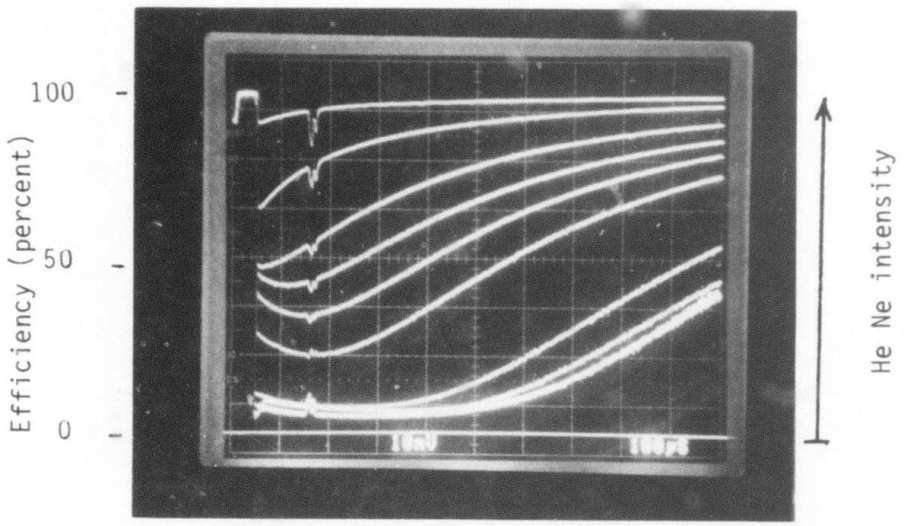

Fig. 2.3 Thermo-optical beam guide efficiency vs. time for several pump pulse energies (one to ten joules in one joule increments). 100 μsec per division.

(a)

(b)

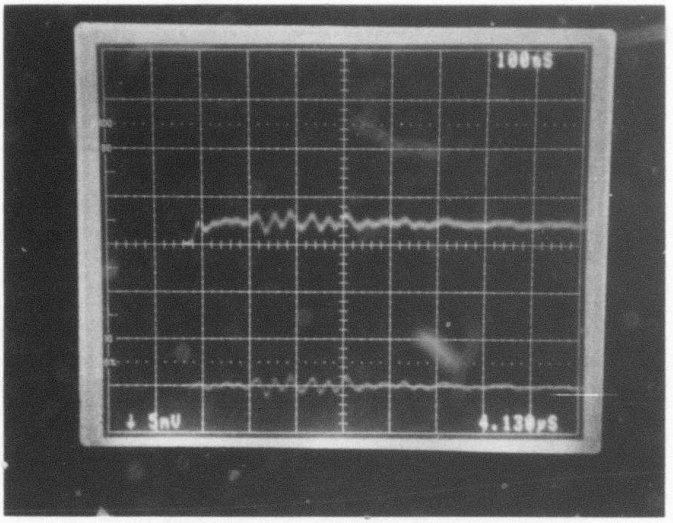

Fig. 2.4 Temporal response for thermo-optical beam guide. 20 nsec risetime is shown in (a). Detector is blocked in (b) and shows RFI noise from pulsed laser electronics. 100 nsec per division.

accurate determination of the risetime, the observed risetime is in general agreement with the expected thermalization time of 10^{-10} sec [14]. As may be seen from Figure 2.3, the stronger laser pulses are more efficient at deflecting the HeNe laser radiation. For the lowest energy pulses, the efficiency is maximum immediately after passage of the exciting green pulse, then decreases nearly exponentially with a time constant of about 0.5 msec as the thermally excited refractive index beam guide thermally diffuses toward equilibrium. The thermal diffusion time t_d for a cylindrical excitation of radius w_o can be approximated using the equation developed in Appendix B

$$t_d = \frac{3w_o^2}{8D}$$

where D is the thermal diffusivity and is on the order of 10^{-3} cm^2 sec^{-1} for liquids ($D = \lambda_T/\rho c_p$ [16]; see Table II). Using a value of 15 μm for w_o we calculate t_d to be 0.84 msec. This is almost twice the measured decay time of 0.48 msec but shows reasonable agreement since the error associated with the measurement of w_o may be significant and the adiabatic assumption in Appendix B may not be totally valid (loss of energy would result in a larger calculated t_d). It also provides us with additional verification that we are indeed observing an interaction of thermal origin.

2.2.2 Deflection Efficiency

It is interesting to note that for the higher pulse energies, the efficiency of the beam guide continues to increase slightly even after the 5 nsec exciting pulse has passed, then falls in an exponential fashion. This slight increase may be explained by the fact that high energy pulses create beam guides possessing large Δn and large ΔT at the center of the guide. As the cylindrical guide expands in its diameter, Δn and ΔT drop in magnitude but since Δn started at a large value, it

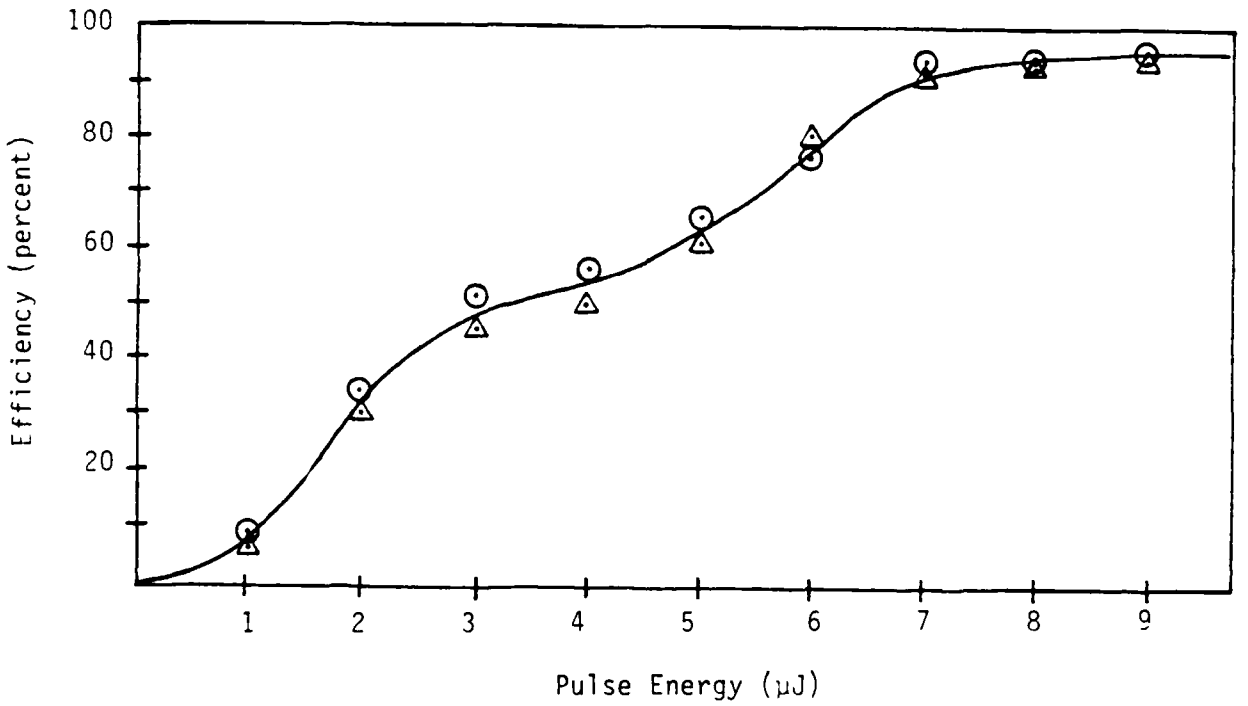

Fig. 2.5 Thermo-optical beam guide efficiency vs. dye laser pulse energy. Different symbols represent two different days.

remains effective in guiding the red beam (see Appendix D). In addition, the larger guide diameter is able to support higher order modes excited by the red beam and is therefore more efficient at guiding the totality of the red beam. Low energy pulses on the other hand will also create guides which increase in size as they diffuse thermally. However, since Δn is smaller to begin with they are less efficient at guiding the red beam, and as Δn drops due to diffusion they become even less efficient at guiding, especially for the higher order modes.

The deflection efficiency as a function of time represented by Figure 2.3 was used to determine quantitatively the maximum deflection efficiency as a function of exciting pulse energy and is shown in Figure 2.5. The efficiency is seen to increase with pulse energy as expected but it is interesting to note a plateau region between 3 and 5 μJ pulse energy. To be sure that an experimental parameter had not changed during the course of the measurements in Figure 2.3, the measurements were repeated on another day. This data is also presented in Figure 2.5 and verifies the presence of a plateau at intermediate energies.

The data presented in Figures 2.3 and 2.5 are for carbon disulfide with iodine as an absorber whose concentration was such that the absorption coefficient at 510 nm was 1.0 cm^{-1}. Similar results were obtained for other liquids and dyes although the efficiencies were lower. Efficiencies at maximum energies of 10 μJ ranged from only a few percent to a maximum of 96 percent. For all liquid-dye combinations, the absorption was adjusted to values near 1.0 cm^{-1} (see Appendix E).

2.2.3 Guiding Mechanism

The observed behavior of the red probing beam passing through the region excited by the passage of the green laser pulse appears to be well-explained by the model of a real-time thermally induced graded index guide (analogous to a GRIN fiber) created within the liquid

sample. The annulus of red light about the green pulse supports this model as does the rapid turn-on of the effect and its slow decay due to thermal diffusion. However, a difficulty arises when one considers the sign of the change in the refractive index.

For a given liquid, the refractive index and density are directly related. We know that the guiding process is thermally driven but it is unlikely that the refractive index depends directly upon temperature. It is most likely that the temperature drives the density which in turn drives the refractive index. That is,

$$\frac{dn}{dT} = \left(\frac{\partial n}{\partial T}\right)_{\rho} + \left(\frac{\partial n}{\partial \rho}\right)_{T} \frac{d\rho}{dT}$$

where the first term on the right is negligible compared to the second term. Since $d\rho/dT$ is proportional to the thermal expansion coefficient, $(1/V)\ dV/dT$, and since dV/dT is a negative quantity for most materials, if the second term is dominant in the above expression then dn/dT is also negative (see Appendix A). Absorption of the green laser pulse leads to an increase in temperature of the liquid which spatially follows the intensity profile of the laser pulse i.e. bell-shaped. However, since the laser pulse is most intense at its center the temperature rise is greatest there and therefore the density and refractive index is expected to be lowest. The refraction index profile is therefore expected to be bell-shaped, but an inverted bell with the lowest index at the center of the beam. This is contrary to most optical waveguides where the refractive index is greatest in the interior (or core) region and lower for the surrounding (or cladding) region thereby relying upon total internal reflection to achieve wave guiding. Although a higher index core is the most efficient for guiding, a lower index core can also lead to guiding and is referred to as a leaky waveguide [23,24] (see Apendix D).

Leaky waveguiding is possible when the refractive index of the interior region of an optical waveguide has a lower value than the exteror region provided that the propagating radiation is near grazing. Upon reflection from the refractive index interface, some of the radiation is transmitted but since the angle of incidence is near 90°, most is reflected at the specular angle, in the forward direction.[1] If the refractive index within our real-time thermally-generate guide is indeed less then the surrounding liquid medium then we conclude that the guiding which we observe is of the leaky mode variety.

To verify that optical heating of the dye-liquid sample leads to a lowering of the refractive index, we placed our sample cell in one of the arms of a Mach-Zehnder interferometer and observed the direction of motion of the fringes when the dye-liquid was heated by a beam of green Ar-ion laser radiation. The laser radiation used in the Mach Zehnder was from a HeNe laser just as the probe in our experiments was from a HeNe laser. Instead of thermally exciting a micrometer sized cylindrical volume in nanoseconds, however, a millimeter sized volume was thermally excited in a second or two using the CW Ar laser beam. The direction of motion of the fringes verified that the refractive index decreased as expected. We therefore conclude that the guiding which we observe is essentially leaky waveguiding.

1/ We note that measurements of guiding efficiency as a function of crossing angle θ resulted in a gradual decrease in efficiency for larger angles. This is consistent with our leaky guide model.

3
THERMAL PHASE GRATINGS

The interference of two coherent beams of laser radiation leads to a sinusoidal intensity pattern which is routinely used to generate holographic diffraction gratings. Transient or real-time phase gratings may be similarly generated by allowing two interfering beams to pass through a nonlinear optical medium whose index of refraction varies with the radiation intensity. These real-time gratings may be used as an optical means of controlling another optical beam for all-optical switching or control functions for optical computers, processors, interconnects, or other applications. We wish to report about the writing of real-time thermal phase gratings in absorbing liquids which were used to switch an optical pulse. The particular switching geometry which was used corresponds to the implementation of an AND gate.

3.1 EXPERIMENTAL

Figure 3.1 shows the experimental arrangement for observing the thermo-optical switching. A nitrogen laser pumped LSI Inc. dye laser whose output is 25 μJ at 0.51 μm in a 5 nsec pulse was used as the radiation source [13]. The laser output was split into two beams of equal intensity which were directed as shown to provide two parallel propagating beams. A Baltar f/2 152 mm lens was used to focus and cross the two beams in their focal volumes. Care was exercised to make the optical path length for the two beams equal to well within the 3mm coherence length of the laser pulse in order to assure a stationary interference pattern of the beams in the focal region. This intensity interference pattern is transformed through absorption of optical energy into a thermal phase grating which occupies the focal region. This process occurs rapidly since thermalization of the absorbed laser energy occurs in times on the order of 10^{-10} sec for liquids [14].

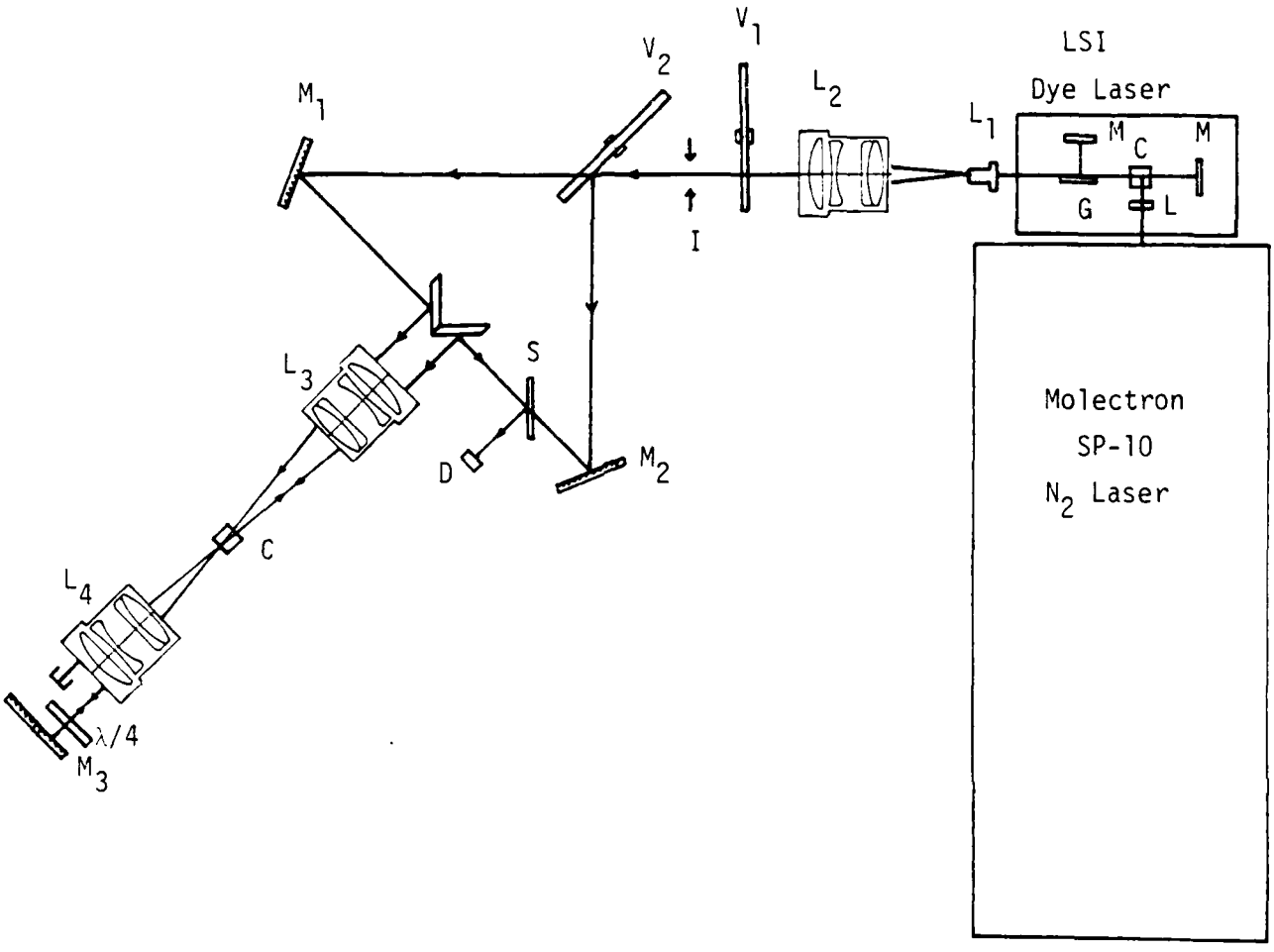

Figure 3.1 Experimental arrangement for phase grating switch.
L: lens; V: variable attenuator/beam splitter;
I: iris; M: mirror; D: detector; C: dye cell;
S: beam splitter; G: grating.

Unabsorbed radiation from one beam which passes through the sample cell is simply blocked while the other beam is reflected by mirror M2 back to the focal region where the phase grating was created. This return geometry is particularly convenient since the Bragg condition is assured when the returning beam is directed through the focal volume.

3.2 RESULTS

Figure 3.2 provides an oscilloscope trace of the signal from the detector in Figure 3.1. The stronger pulse with the fast risetime represents the incident laser pulse and was obtained by removing the blocker in Figure 3.1 and placing it in front of the quarter wave plate. The lower intensity, more rounded pulse is the radiation which was switched by the thermal phase grating generated in the sample. Using 10 μJ laser pulses and a sample of carbon disulfide with iodine as the absorber (0.3 cm^{-1} absorption) the peak efficiency was measured to be 15 percent. Carbon tetrachloride, ethanol and methanol with iodine, eosine or cobalt chloride were also used with similar, although slightly less efficient, results.

It should be noted from the oscilloscope traces of Figure 3.2 that the onset of the switched radiation is delayed in time by about 2 nsec. This time delay is in quantitative agreement with that expected for equilibration of a thermally induced pressure disturbance propagating at the speed of sound over a 3μm distance corresponding to the grating wavelength and is discussed in Appendix C.

Verification that the reflected probing radiation was Bragg reflected by the phase grating created by interference of the two incident beams was indicated by blocking one or the other of the incident beams in Figure 3.1. When either beam was blocked, the signal to the detector disappeared. This experimental geometry is functioning as a three-port AND gate. If radiation is present in both input beams A

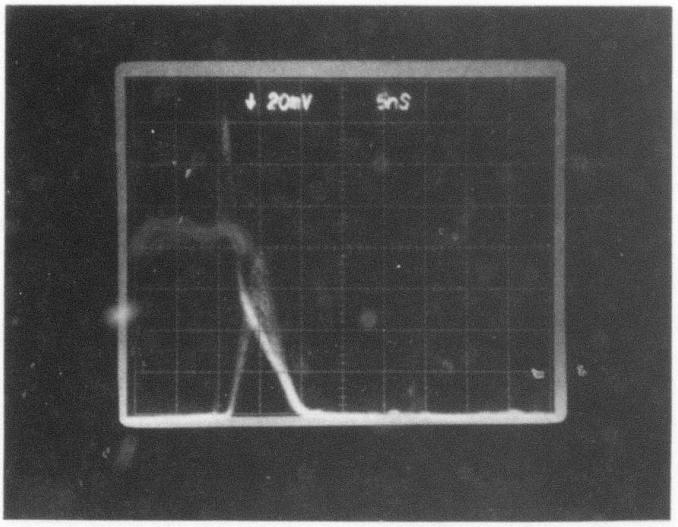

Fig. 3.2 Temporal response for thermo-optic phase grating. Strongest pulse represents the incident dye laser pulse. The bell-shaped pulse is the radiation diffraction from, or switched by, the phase grating (note the 2 nsec delay). 5 nsec per division.

AND B then radiation will be present in the output C to the detector. Implementations of other logic functions are discussed in Section 3.4 below.

3.3 THERMO-OPTICAL INTERACTION

A simple model may be used to quantitatively determine the switching efficiency as well as the temperature rise, refractive index change and temporal relaxation of the observed thermo-optical interaction. If E is the energy contained in each of two interfering pulses focused in an absorbing liquid, and w_o is the $1/e^2$ intensity waist radius of the focal region, then the average rise in temperature due to a single beam is [13]

$$T = \frac{\alpha}{\rho C_p} \frac{E\, e^{-\alpha z_f}}{2\pi\, w_o^2} \tag{3.1}$$

where α is the absorption coefficient of the material medium, z_f is the propagation distance to the focus, ρ and C_p are the density and specific heat, respectively, for the medium, and r is the distance from the axis of the beam to any point in the focal volume. Interference of two equal intensity beams leads to a spatially sinusoidal temperature profile where

$$\Delta T = T_{max} - T_{min}$$

$$= \frac{2\alpha}{\rho C_p} \frac{E\, e^{-\alpha z_f}}{\pi\, w_o^2} \tag{3.2}$$

If the two beams are not equal then E should be replaced by $\sqrt{E_A E_B}$ where E_A and E_B are the energies in the two beams, respectively. The resulting refractive index change is (see Appendix A)

$$\Delta n = \frac{dn}{dT} \Delta T$$

$$= \frac{(n^2 - 1)\ (n^2 + 1)}{6n} \beta_v \Delta T \qquad (3.3)$$

where β_v is the volume thermal expansion coefficient for the liquid and where we have assumed the Lorentz-Lorentz law to be valid for relating refractive index and density. The diffraction efficiency for such a reflection phase grating or hologram is [21]

$$\eta = \tanh^2 \left[\frac{2\pi\ w_o\ \Delta n}{\lambda_o \sin \phi}\right] \qquad (3.4)$$

where λ_o is the vacuum wavelength of the (read) radiation and ϕ, the (internal) angle between the radiation propagation vector and the grating fringe planes, satisfies the Bragg condition. (If the read and write wavelengths are equal then $\phi=\theta/2$.) Determination of the experimental parameters E, α, z_f, ϕ and w_o as well as the material parameters of the liquid medium β_v, ρ, C_p and n allows one to compute the diffraction efficiency.

The beam waist radius, w_o, is the parameter with the most error associated with it. If the laser beam is a lowest order TEM_{oo}, Gaussian beam, w_o may be calculated using

$$w_o = \frac{\lambda_o f}{\pi w} \qquad (3.5)$$

where w is the $1/e^2$ intensity radius of the beam before it is focused by a lens of focal length f. The value of w_o used in our experiments was measured by projecting the interfering beams onto a screen (see Figure

3.3) using a lens positioned at the rear of the sample cell. Calculating the spacing, Λ, of the interference fringes

$$\Lambda = \frac{\lambda_o}{2\, n \sin \phi'} \tag{3.6}$$

where ϕ' is the measured exterior half-angle between the two interfering beams, one may simply count fringes and multiply by Λ to determine w_o. This experimental technique is also valuable in providing verification of interference of the two beams in tne focal volume, thereby assuring equality of the path length to within a coherence length.

For incident beams having an energy E of 10μJ each, focused a distance z_f = 0.5 cm in carbon disulfide containing iodine dye in a concentration necessary to provide an absorption coefficient α of 0.3 cm^{-1}, the beam waist radius w_o was measured as 15 μm and, using the liquid parameters of Table II, a temperature rise T of 0.14°C was calculated. The interference pattern should therefore lead to a thermal grating with a peak-to-peak temperature difference ΔT of 0.55°C. This corresponds to a phase grating with a peak-to-peak refractive index difference Δn of 3.7×10^{-4} and, for an interior beam crossing angle θ' of 7°, an expected diffraction efficiency η of 26 percent is computed as shown in Figure 3.4. This is in reasonable agreement with the 15 percent efficiency observed in Figure 3.2.

3.3.1 CW Probe

Additional experiments were performed which probed the phase grating produced by the two interfering pulses using a continuous wave CW laser beam. A constant CW probe should allow an accurate experimental determination of the creation and decay times for the phase grating. Analysis shows that the decay for a thermal grating is exponential with a time constant equal to (Appendix B)

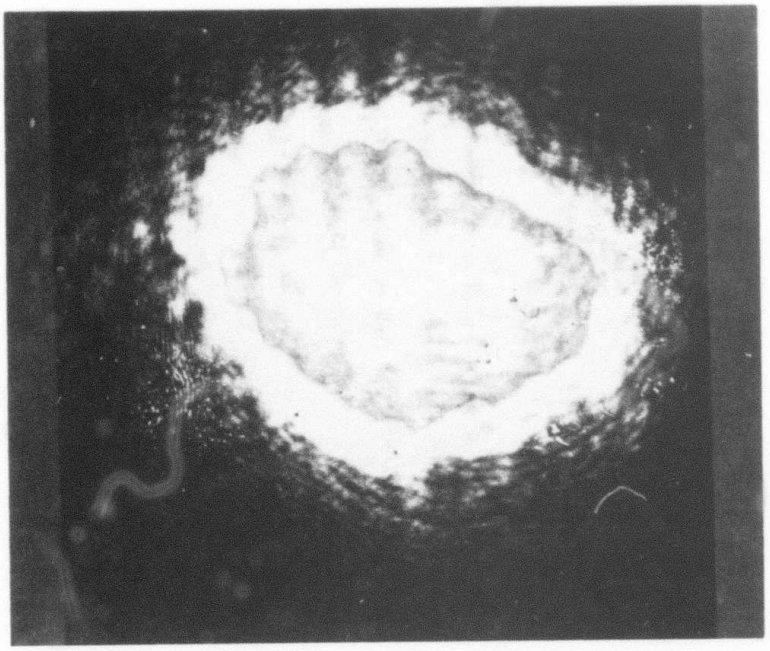

Figure 3.3 Interference pattern of two crossing laser beams in the focal region of a 152 mm lens. The fringe spacing is 3μm.

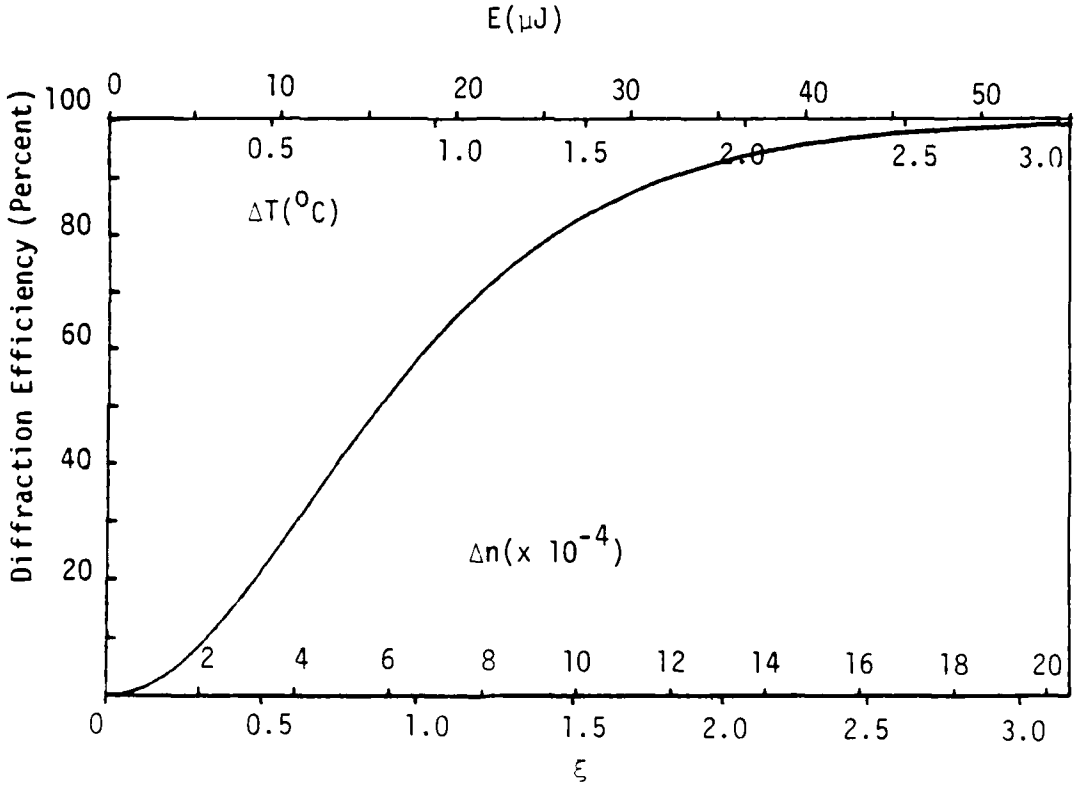

Figure 3.4 Computed diffraction efficiency, η, for a thermally induced thick reflective phase hologram.

$$\eta = \tan^2(\xi), \text{ where } \xi = \frac{2\pi w_o \Delta n}{\lambda \sin \phi} .$$

$$t_d = \frac{(\Lambda/2\pi)^2}{D} \tag{3.7}$$

where Λ is the spatial periodicity of the grating and D is the thermal diffusion coefficient for the host liquid. For the conditions of our experiment of a 7° internal crossing angle ($\theta = 3.5^{o}$), Λ is $10\lambda_o/n$, and D is approximately 10^{-3} cm^2sec^{-1} for liquids, so that we expect a decay time of about a μsec. This is several orders of magnitude faster than for our beam guiding experiments but several orders of magnitude slower than for STRS or where θ is large (see Table III).

First attempts at using a cw probe were performed using radiation at 632.8 nm from a Spectra Physics model 125 HeNe laser. Since the pumping wavelength for writing the grating was 510 nm, the red probe radiation must follow a different path to the focal region where the phase grating is created in order to satisfy the Bragg condition for the diffraction process. This makes the alignment more difficult than when using the pulsed probe derived from the pump radiation. These experiments were unsuccessful and no diffracted red radiation was observed. Computations showed that care must be exercised in assuming that the red probe be at the Bragg angle to within $\pm$ 3 mrad in order that the diffraction efficiency not be degraded (Appendix H).

The difficulties in this experiment were due to: (1) critical alignment of the probe through the 30μm diameter focal region, (2) probing at the proper Bragg angle, (3) milliwatts of CW probe power vs watts of pulsed probe power, and (4) thermal effects due to the probe energy .[2] Difficulties (1) and (2) can be effectively eliminated by going to a CW probe at the same wavelengths as the pump radiation and being sure that they follow the same path. This does however exacerbate

---

2/ (CW: mw x μsec = nJ; pulse: w x nsec = nJ).

Table III

Characteristics for Thermally-Induced Optical Interactions

	Dimension (d)	Rise Time (t_r)	Decay Time (t_d)
Beam Guiding*	100λ; $30\mu m$	10^{-8}s	10^{-3}s
Phase Grating**	10λ; $3\mu m$	10^{-9}s	10^{-6}s
STRS	$\lambda/2$; $0.15\mu m$	10^{-10}s	10^{-8}s

*Thermal Gaussian cylinder with $1/e^2$ diameter d

$$t_d = \frac{1}{D}\left[\frac{d}{2\pi}\right]^2$$

** Thermal sinusoidal grating of spacing d

$$t_d = \frac{3}{32}\frac{d^2}{D}$$

D is the diffusion coefficient which is, for liquids, approximately 10^{-3} cm^2 sec^{-1}.

(4) since the probe wavelength is now substantially absorbed.

An argon ion laser beam at 514.5 nm was used as a probe beam and the dye laser pump was tuned to the same wavelength. Although care was exercised to align the CW probe beam through the interaction region where the grating was produced, no diffraction was observed. Any of the aforementioned difficulties, except the Bragg angle, could be the cause. At these low probe powers we may simply not have an adequate signal to noise ratio to see the deflected radiation with our detection system. Time constraints for the program did not allow us to pursue this further.

3.3.2 Phase Conjugation

It should also be noted that the experimental geometry of Figure 3.2 is similar to that used for performing degenerate four-wave mixing, DFWM, experiments [22]. In DFWM, beam A and beam B reflected from M2 are considered the pump beams, beam C is now the phase conjugation probe, and beam D would correspond to the phase conjugate of C. DFWM entails three interactions which result in a phase conjugate beam. Two of these are holographic interactions occurring in real-time while the third is a breathing-mode interaction [22]. All three interactions require mutual coherence between the three input beams in the overlap region. Our experiment satisfies the coherence requirement between beams A and C but the additional path length to the mirror M2 and back for beam B makes it unacceptable for generating a grating or hologram but acceptable as the reading beam for the hologram produced by the interference of beams A and B. In addition, the use of a double-passed quarter-wave plate renders the beam C orthogonal to both beams A and C and precludes any interference effects with their fields. As such, we can expect to see manifestations of phase conjugation in our experiment but only those resulting from one of the two real-time holographic

terms. Time did not permit the experimental verification of the phase conjugation.

3.4 OPTICAL CONTROL

The switching which was demonstrated using the thermo-optical phase grating discussed in Section 3.2 is essentially an AND gate. Implementation of other geometries allows for the other logic functions of OR, and XOR. The XOR gate may be used as an inverter which, in conjunction with the AND and OR gates, results in NAND and NOR gates, respectively. The AND gate geometry may also be used as an amplifier to couple energy from one beam into that of another and may be used as an optical clipper or limiter.

3.4.1 Logic Gates

Table IV summarizes the different logic functions

AND

Figure 3.5(a) shows schematically the thermo-optical phase grating demonstrated in this program which functions as an AND gate. A and B are the inputs and D is the output. If either A or B are zero, then no phase grating can be formed and there is no output at C. If both A and B are "on" then a phase grating is formed in their crossing region and A radiation which is reflected by the minor M is diffracted by the grating to become the output at C. The throughput on efficiency of the gate is improved by assuming the radiation in both inputs is polarized in the plane of the figure and a quarter wave plate is used to rotate the plane of polarization of beam D to be perpendicular to the plane of the figure so that the reflection from the beam splitter (preferably a polarizing beam splitter) is increased.

Table IV
Logic Gates

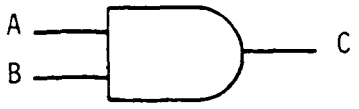

A	B	C				
		AND	OR	XOR	NAND*	NOR**
0	0	0	0	0	1	1
1	0	0	1	1	1	0
0	1	0	1	1	1	0
1	1	1	1	0	0	0
		$A \bullet B$	$A+B$	$A \oplus B$	$\overline{A \bullet B}$	$\overline{A+B}$

* NAND = NOT + AND

** NOR = NOT + OR

NOT ≡ Inverter

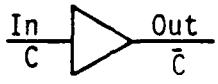

In - C	Out - $\bar{C}$
0	1
1	0

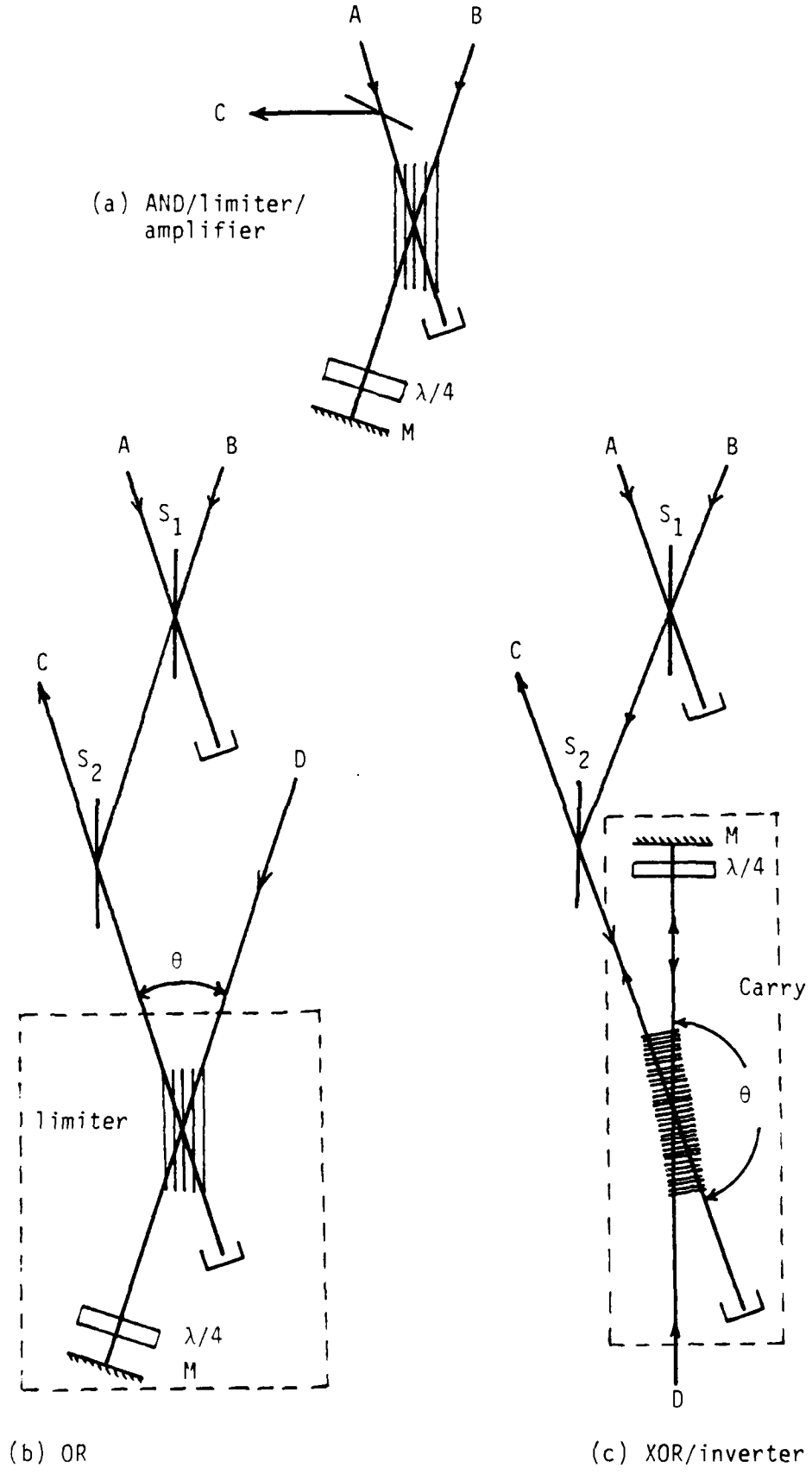

Fig. 3.5 Optical implementation of logical gates. A and B are the inputs, C is the output and D is a constant pump source.

OR

A 50:50 beam splitter by itself as shown in the top portion of Figure 3.5(b) is very close to being an OR-gate. A zero for both A and B results in zero output from the beam splitter. If either or both of A or B is "on" then there is an output. The difficulty lies in the fact that the output for both inputs "on" is twice that for only one input "on". This can be remedied with the use of an optical limiter as shown in the bottom of Figure 3.5(b). If beam D is of adequate intensity, (and temporally coherent with both A and B), then a reflection grating can be produced by the nonlinear optical interference between the output from S, and beam D. Radiation from beam D which is folded back by mirror M is reflected by the phase grating whose transfer characteristics are that of a hyperbolic tangent squared as discussed in Section 3.3. If Δn, which is proportional to the product of their intensities), is large enough so that the diffraction efficiency of the grating is near unity, then the output C is the same whether the beam from S_1 is single or double leveled.

XOR

The exclusive-OR gate, or XOR, is implemented in a similar fashion to the OR gate using a beam splitter but replacing the limiter with a carry as shown in Figure 3.5(c). The nonlinear optically induced phase grating due to interference between the input beam to the inverter and beam D, has a periodicity on the order of $\lambda/2$ since θ is nearly 180^{o}, and behaves as a reflection grating for radiation reflected by mirror M. Since the transfer function of a reflection grating (hologram) is a sine-squared function, as shown in Figure 3.6(b), if beam D is set for the proper intensity, the presence of beam A or B alone produces a reflectivity of near unity whereas the presence of both A and B doubles the Δn to produce a reflectivity of near zero.

NAND

The Not-AND, or NAND, gate can be implemented using an AND gate followed by an inverter.

NOR

The Not-OR, or NOR, gate can be implemented using an OR gate followed by an inverter.

3.4.2 Inverter/NOT

The XOR gate with the B port always "on" results in an inverter, or NOT gate, with A as the input and C as the output.

3.4.3 Clipper/Limiter

The thermo-optical switch which was demonstrated during this program and whose structure is shown in Figures 3.1 and 3.5(a) can also serve as an optical clipper or limiter. Since the transfer function for such a switch is a hyperbolic tangent (Figure 3.6(a)), and since the argument is proportional to the square root of the product of the two input intensities (see Equation (3.9)) if the input to the B-port is strong enough, then inputs to the A-port above a certain value results in a near-unity reflectivity phase grating. The output of the device is linear with respect to the input (and is amplified - see below) for small inputs. For larger inputs, the output slowly saturates and for still larger inputs the output energy is fixed or limited.

3.4.4 Amplifier

Two techniques for achieving gain or amplification can be implemented using the phase grating approach.

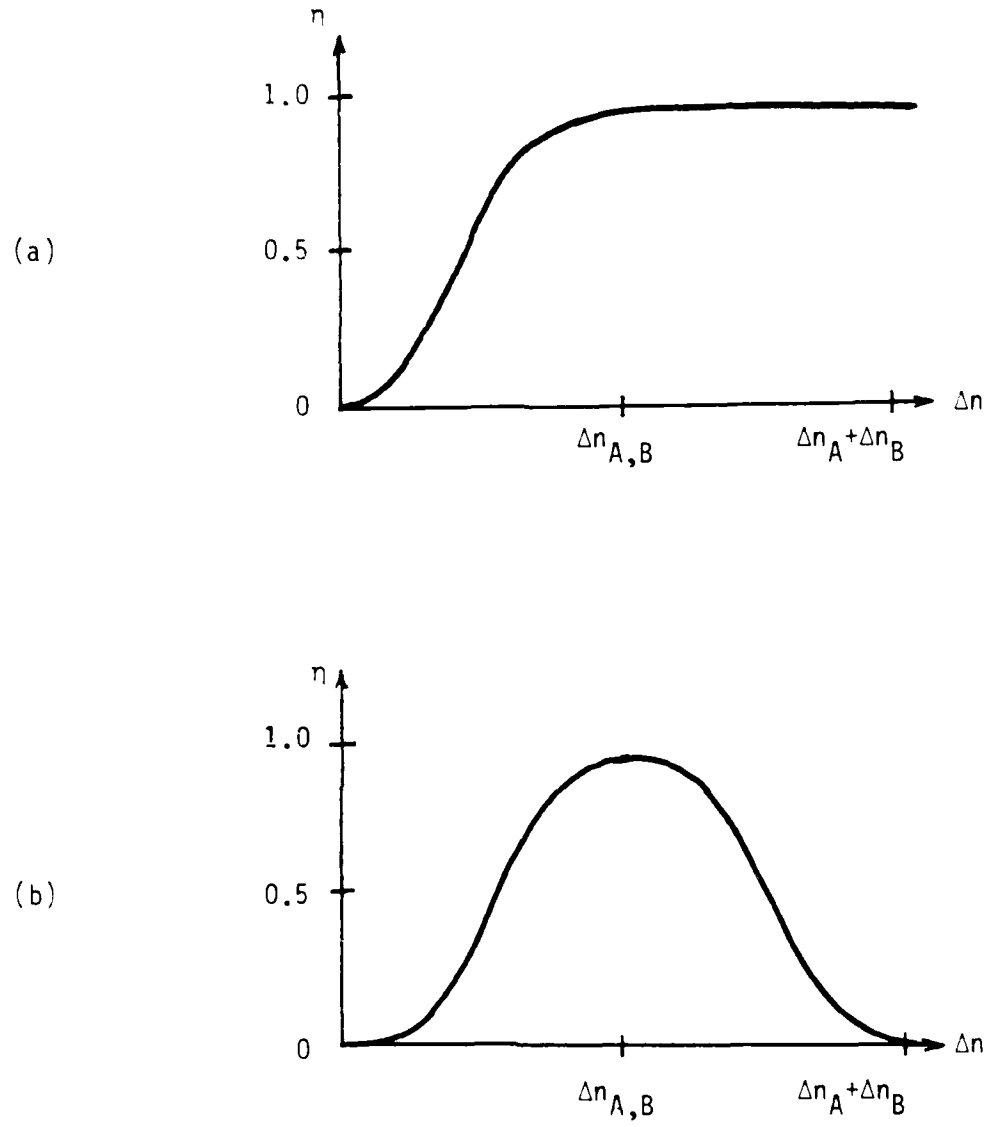

Fig. 3.6 Phase hologram diffraction efficiency versus refractive index amplitude. (a) Reflection phase grating - $\tanh^2$. (b) Transmission phase grating - $\sin^2$.

3.4.4.1 Stationary Phase Grating

The thermo-optic phase grating shown in Figure 3.1 can serve not only as an optically controlled on-off switch, AND gate, and optical limiter, but also as an optical amplifier. If the input to the A-port in Figure 3.5(a) is of adequate intensity then an input signal in the B-port leads to the creation of a phase grating in the region where they cross.

For crossing angles which are small (c.f. Figure 3.5(a)), the grating spacing is large and the grating behaves as a reflection hologram whose diffraction efficiency is [21]

$$\eta = \tanh^2 \left[\frac{2\pi w_o \Delta n}{\lambda_o \sin(\theta/2)}\right] \tag{3.8}$$

$$\Delta n = \frac{dn}{dT} \frac{2\alpha}{\pi C_p} \frac{\sqrt{E_A E_B}\, e^{-\alpha z_f}}{\pi w_o^2} \tag{3.9}$$

where E_A and E_B represent the energy in the optical beams serving as input beams to posts A and B, respectively, and where the other parameters in the equations are defined in Section 3.3. E_A can be considered as a function of time

$$E_A(t) = \pi w_o^2 I_A \int_0^t \varsigma(t')dt$$

where I_A is the peak intensity of beam A and $\varsigma(t')$ is the pulse-shape function. $E_B(t)$ may be expressed similarly. For crossing angles which are large, approaching 180^o (θ in Figure 3.5(c)), the grating spacing is

small and on the order of $\lambda/2$. Here, the grating behaves as a reflection hologram whose diffraction efficiency is [21]

$$\eta = \sin^2\left[\frac{2\pi w_o \Delta n}{\lambda_o \cos\theta/2}\right].$$

When the argument for the diffraction efficiency is small compared to one, both $\tanh^2$ and $\sin^2$ functions become

$$\eta \pm \left(\frac{2\pi w_o \Delta n}{\lambda_o \sin \psi}\right)^2$$

where ψ is equal to $\theta/2$ for the transmission hologram and equal to $(\pi - \theta)/2$ for the reflection hologram case.

If η is the grating diffraction efficiency and $K_A I_A$ (where $K_A \lesssim 1$ is a proportionality constant) is the radiation reflected by the mirror in Figure 3.5(a), then the diffracted radiation is equal to

$$I_C' = \eta(K_A I_A)$$

where I_C' is the intensity of the output radiation in beam C before it is reflected by the beam splitter. (We assume $I_C = K_C I_C'$ where $K_C \lesssim 1$). The output, I_C, may therefore be written as

$$I_C = \beta I_A^2 I_B,$$

where

$$\beta = K_A K_C \left(\frac{2\pi w_o}{\lambda_o \sin\psi}\right)^2 \left[\frac{dn}{dT} \frac{2\alpha}{\rho C_p} e^{-\alpha z_f} \int_0^t S(t')dt'\right]^2,$$

if we assume that the pulse shape factors are the same for both A and B. If I_A^2 is large enough such that βI_A^2 is greater than unity, then I_C is an amplified version of I_B.

The integral of the pulse shape factor in β is a result of the assumption that the time history of the pulse shape is fast compared to the decay time for the nonlinear medium and is proportional to the pulse energy up to time t. For rapid time decays which are less than the temporal structure in the laser pulse, the integral can be replaced by $\varsigma(t)t_d$ where t_d is the decay time. The amplification process (and also the limiting action) therefore acts upon the instantaneous laser intensity or power rather than upon the energy, but more total energy is required to accomplish this action.

3.4.4.2 Moving Phase Grating - Two Wave Mixing

Throughout the bulk of this report, it is assumed that the interfering beams which create the phase gratings are coherent with respect to each other and possess the same optical frequency. This is easily accomplished by deriving the beams from the same source and being sure that the optical path lengths from the source to the interference region are the same to within a coherence length. If this is done properly the interference fringes will have good contrast and will be stationary in space.

If however, the two interfering beams are coherent with respect to one another but one has a frequency offset (for example due to the Doppler shift from an acousto-optic beam deflector), then the interference fringes will again have good contrast but will move in space in a direction perpendicular to the fringe planes. If $\Delta\nu$ is the optical frequency difference and Λ is the fringe spacing, then the time required to move one complete fringe is (c.f. heterodyne detection)

$$t_\Lambda = \frac{1}{\Delta\nu} ,$$

and the fringe velocity is

$$V = \Lambda \, \Delta s$$

$$= \frac{\lambda \, \Delta\nu}{2\sin(\theta/2)}$$

If t_d is the time for a thermal disturbance to decay and if t_d is greater than t_Λ then the phase grating lags behind the fringes and the phase grating is washed out for laser pulses whose duration exceeds t_Λ. If however t_d is less than t_Λ then the phase grating follows the fringes as they move. If t_Λ happens to equal t_d then the phase grating will lag behind the moving fringes but is not totally washed out. The phase grating is retarded by approximately one-half wave compared to the thermally exciting fringe pattern.

Consider for a moment a stationary phase grating formed by two interfering beams A and B as shown in Figure 3.5(a). Once the phase grating is formed, it is reasonable to expect that a fraction (η) could be diffracted from one beam into the other beam. If A is much greater than B, one might reason that B should increase at the expense of A. Closer examination of the interaction however shows that the diffracted waves are 180^o out of phase with respect to the waves in the straight-through beam. If the phase grating was shifted by one-half of a period, or $\Lambda/2$, compared to the fringe pattern then the diffracted wave is in phase with the straight-through beam and coupling can occur from one beam to the other. This shift is built in to the space charge distribution for optically induced gratings in photofractive crystals, and is the basis for beam coupling or energy transfer using these crystals and is referred to as two-wave mixing [30].

Two wave mixing may also be facilitated using thermo optical phase gratings by properly matching the decay time of the thermal grating with the motion of the grating. If the experiment is designed to match t_Λ to t_D, by choosing the appropriate $\Delta\nu$ and Λ, so that

$$t_\Lambda = t_d,$$

then the phase grating is retarded or shifted in space by one-half wave or by $\Lambda/2$. This results in the desired 180^o phase shift of the diffracted radiation so that both the straight-through and diffracted waves are in-phase. Two-wave mixing whereby energy from one (strong) beam is coupled to that of another (weak) beam can be achieved by crossing the two beams and providing the appropriate frequency off-set. Table III and Figure 4.1 show that for small crossing angles, t_d is on the order of milliseconds such that $\Delta\nu$ needs to be on the order of kHz. This is such a small frequency offset as to be much smaller than the laser radiation linewidth. As such, there will be as many positive frequency offsets as negative frequency offsets such that energy is equally coupled from beam A to B as from beam B to A.

If the angle θ is large, approaching 180^o, t_d is on the order of 10^{-8} such that $\Delta\nu$ is on the order of 100 MHz. This is a reasonable frequency shift for conventional acousto-optic beam deflectors and should be achievable in the laboratory. It is worth noting that it is precisely this same mechanism that is responsible for the amplification observed in stimulated thermal Rayleigh scattering which is observed in backscattering where $\theta = 180^o$.

3.5 PARALLEL ARRAYS

Although the implementation of a single switching element is an important first step, in order to take advantage of the parallelism available for optical systems, the switching method must be amenable to

incorporation into a two dimensional array. Figure 3.7 provides an architecture for obtaining amplification, clipping, and logical AND for a 3 x 3 element array. Coherent laser radiation is incident from the left where it encounters two equivalent holograms which angularly multiplex the beam. The output from each hologram is several collimated beams whose propagation vectors differ from each other (in two-dimensions) by a fraction of a milliradian. When focused by the first lenses a 3 x 3 array of foci separated by a few tens of microns are located in the focal plane. Input information may be placed in the A and B arrays using fixed masks or dynamic spatial light modulators (SLM's). Each beam is recollimated and focused with a single focusing lens. Since each element in one beam has a matched propagation angle in the other beam they will cross in the focal plane at spatially separated positions. For each element of the array, if both the A and B contribution are in the "on" state (i.e. finite transmission at the mask), then the two beams interfere to create, in the presence of a nonlinear medium, a spatial phase grating. The A-radiation is folded back to probe the focal volume using the retroreflector. For a given element, if both A and B are "on" then the grating diffracts radiation to the output beam splitter and focusing lens. The resulting 3 x 3 array represents A AND B for the case of a mask at both A and B. The output represents an amplified B array if A has no mask but is a fixed intense beam and B is a weak signal array. The output is a clipped or limited array if A has no mask and is a fixed intense beam and B is strong enough to lead to saturation of the generated phase grating. Mixtures of all three optical function could be incorporated in a single mask structure.

A 3 x 3 array size was chosen for ease of discussion but larger n x n arrays would function similarly. Average optical power becomes a consideration for large arrays and high repetition rates. If switching is performed at a MHz rate and 10μJ is required for a thermo-optical switch, then 10 watts of average optical power is needed and

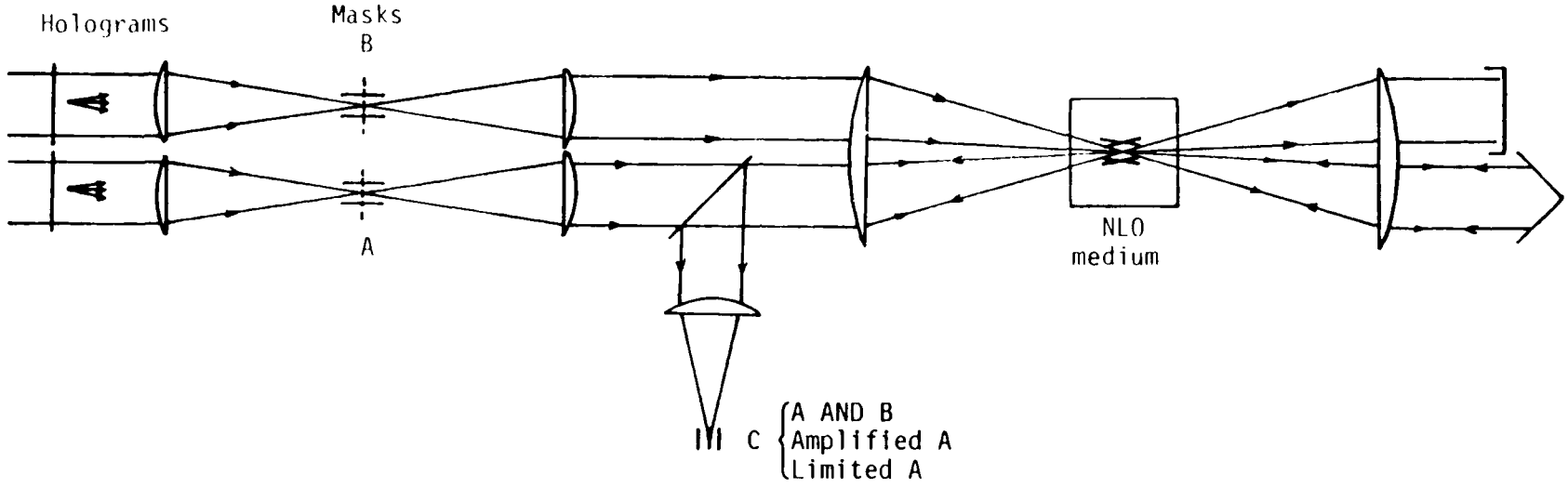

Fig. 3.7 Two-dimensional implementation of AND gate, amplification or limiting. Input arrays are in masks A and B, and output is at C.

approximately one watt is absorbed by the medium as heat. For a modest 10 x 10 array, a 1Kw average power pulsed laser is needed and 100 watts of heat is generated. Although the phase grating is amenable to a parallel architecture, the 10μJ which may be necessary for a single thermo-optic switch appears to be excessive and needs to be reduced by orders of magnitude.

4
DISCUSSION AND CONCLUSIONS

The primary thrust of this research effort has been to investigate and explore thermo-optical interactions as a means for achieving all optical control functions. To this end, we have demonstrated laser beam control by (1) beam guiding and (2) thermal phase gratings.

The beam guiding entails the creation of an optical beam guide or real-time "fiber" by the passage of a focused pulse of laser radiation through an absorbing medium. Radiation from a second laser beam can be coupled into and guided by the thermally induced refractive index guide in switching times on the order of nanoseconds. The guide persists for durations which are determined by the thermal diffusion times of the absorbing medium. For the liquids used in the reported experiments, and for the dimensions involved, the persistence is on the order of a millisecond and is shown to be in reasonable quantitative agreement with the thermal model presented. Since the switch-on time to create the guide is on the order of nanoseconds, it is reasonable to expect that another laser pulse could be used to destroy the guide in a comparable time to produce a rapid switch-off time. This was not demonstrated in the program however.

The energy required to produce the beam guiding is modest and is on the order of microjoules. The experimental parameters are found in Table V. The laser induced guide could function as an on-off switch for a second beam of radiation or as an optical means for redirecting the radiation in a second laser beam. Although the switched laser radiation is distributed into an annular cone of light, a simple lens is able to focus the radiation down to a single spot.

Although the results of the beam guiding experiments are well explained by the thermal model, a difficulty is encounted with the sign of the thermally-induced refractive index change. Absorption of the laser energy in the cylindrical focal region leads to an increased temperature there. A rise in temperature is expected to produce a decrease in the density and therefore a decrease in the refractive index in the cylindrical focal region. Guiding by total internal reflection requires that the guide possess a higher refractive index than for the surrounding medium. If the thermally-induced guide region has a lower refraction index than its surroundings, as was verified by interferometer experiments, then the beam guiding must be attributed to a leaky mode.

Optical-optical laser beam control using a thermo-optically generated phase grating was also investigated and demonstrated. The interference of two laser pulses at a crossing angle of 7^{o} was used to create a phase grating having a 3 μm spatial period in a time of 2 nsec and is in agreement with the thermal model. The experimental parameters are found in Table V. The thermal model predicts a decay time of 4 μsec for the grating but was not measured due to experimental difficulties. For 10 μJ laser pulses, the diffraction efficiency for the grating was measured as 15 percent and was in reasonable quantitative agreement with the model which specified a thermo-optic grating having a 0.55^{o}K thermal amplitude, a 3.7×10^{-4} refractive index amplitude, and a predicted diffraction efficiency of 26 percent.

The two switching techniques which were experimentally demonstrated during this program, utilizing real-time generation of beam guides and phase gratings, are very different in principle yet have many features in common. They both are thermal in origin and appear in absorbing media where the absorption coefficient is approximately equal to the reciprocal of the length of the optical path through the absorbing medium. Their turn-on times are proportional to the characteristic

Table V

Experimental Parameters for Thermo-Optical Beam Guide and Phase Grating

	Guide	Grating
Pulse energy, E	$10\mu J$	$10\mu J$
Pulse duration, t_p	5nsec	5nsec
Wavelength, λ	510nm	510nm
Crossing angle (internal), θ	7^o	4^o
Grating spacing, Λ	-	$3\mu m$
Distance to focus, z_f	0.3cm	0.5cm
Focus diameter, d	$30\mu m$	$30\mu m$
Absorption coefficient, α	$3cm^{-1}$	$0.3cm^{-1}$
Temperature difference, ΔT	0.64^oC	0.55^oC
Index difference, Δn	$4.3x10^{-4}$	$3.7x10^{-4}$

	meas.	calc.	meas.	calc.
Deflection efficiency, η	96%	-	15%	26%
Risetime, t_{rise}	20ns	15ns	2ns	1.5ns
Decay time, t_{decay}	0.5ms	0.84ms	-	$4\mu s$

transverse dimension of the excitation divided by the acoustic velocity of the medium. For a beam guide this characteristic dimension is the laser beam diameter itself while for the phase grating it is the grating spacing. For micrometer dimensions, the switch-on times are on the order of 10^{-9} sec.

The persistence of these thermo-optical switches is limited by thermal diffusion. The decay time is proportional to the square of the characteristic dimension and inversely proportional to tne diffusion constant. If long times, or memory, is desired, the beam guide persists for times on the order of a millisecond. For shorter times, on the order of a microsecond, the grating approach may be used. By changing the angle of interference which produces the grating, several orders of magnitude of decay times can be covered as shown in Figure 4.1. The thermal-optical switching can be fast, can have memory associated with it, and can be achieved at microjoule levels of optical energy.

It is commonly felt in the scientific community that thermo-optic effects possess strong optical monlinearities but are slow. Indeed, they cannot compare with optical nonlinearities whose origins lie in the electronic polarizabilities of molecules whose response times are nearly instantaneous and are on the order of femtoseconds. Thermal effects are however, not as slow as is commonly depicted in the literature [31,22] where typical response times for thermal effects are presented as being in the range of 0.1 to 1.0 sec. We have observed thermo-optic response times to be in the nanosecond range and for other geometries should go into the sub-nanosecond range also.

On-off switching and the redirection of an optical beam by optical means was demonstrared in this program using thermo-optical beam guiding and phase grating approaches. An AND gate was also demonstrated experimentally using the phase grating approach. Extension to the other logical gates as well as the implementation of optical inverters,

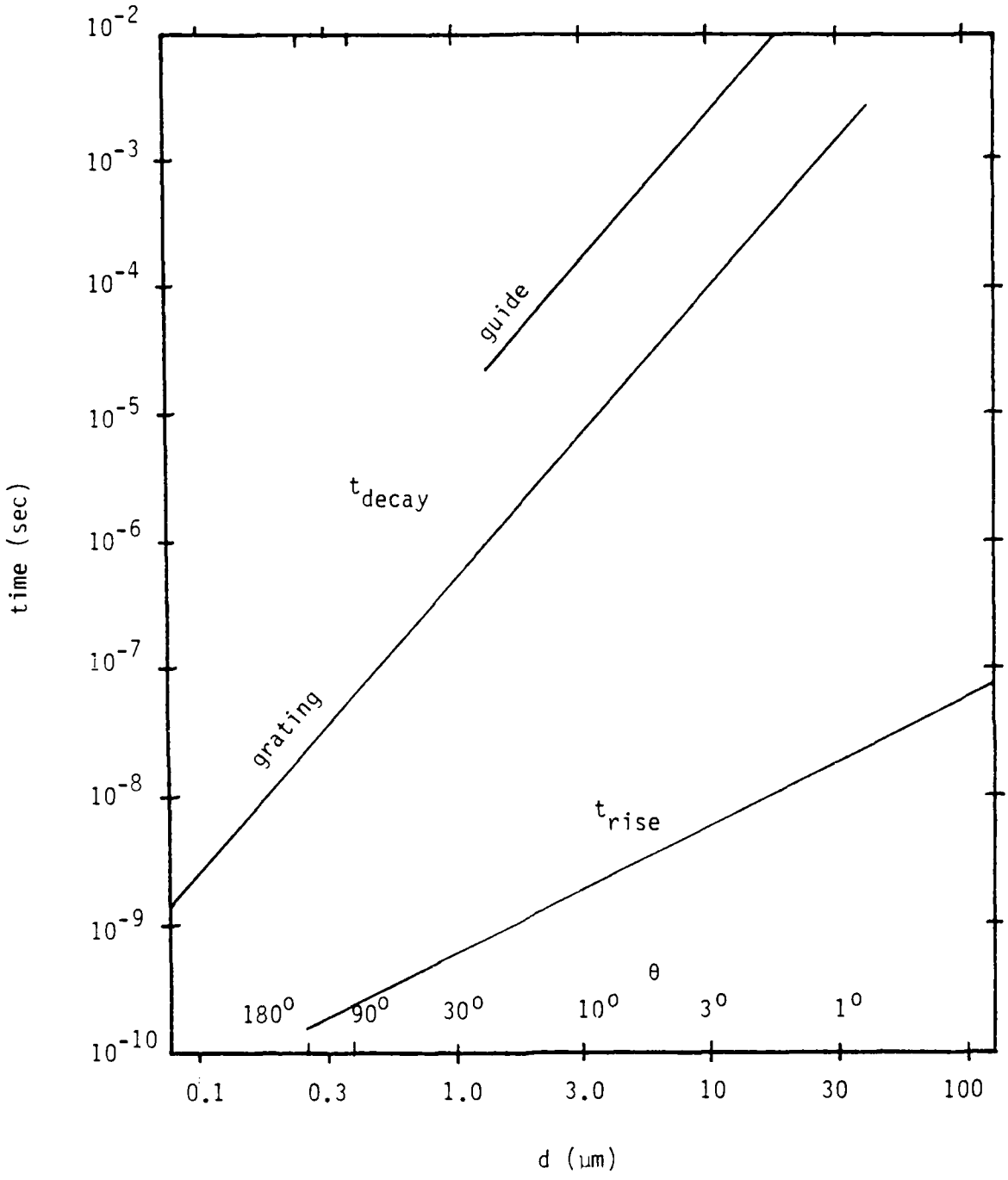

Fig. 4.1 Thermo-optical response times in liquids as a function of characteristic dimension d. For beam guiding, d represents the beam diameter; for the phase grating, d represents the grating period. θ represents the (external) angle necessary to achieve a grating period d; λ = 0.5 μm.

clippers and amplifiers appears to be straight forward. Extension of these single optical elements into arrays of elements to fully take advantage of the parallelism offered by optics is also straight forward. However, the microjoule levels required to switch a single element leads to high power requirements and significant heat dissipation when multiple elements and rapid switching rates are projected. Clearly there must be improvements in reducing the energy required for switching a single element.

5
RECOMMENDATIONS

Based upon the knowledge gained from the analysis and experiments conducted during the course of this program, the following recommendations are provided.

An important area for further study addresses the issue of achieving optical control with lower energy requirements. This is necessary in order to achieve reasonable operation of many parallel channels, and switching at useful repetition rates. Although innovative changes in the experimental geometry may lead to improvements in these energy requirements, the greatest improvements can be expected in alternate materials and/or operating points which possess greater efficiency. For example, a single fluid or a binary mixture exists near a critical point such that a minor perturbation in temperature leads to a phase transition, extremely high scattering can result and is referred to as critical opalescence. It may be possible to write thermally-induced gratings in such media using modest energy while obtaining high diffracting efficiency. Also, semiconductor filter glasses possess sharp band edges which are shifted by small changes in temperature and may similarly be used as a medium for writing the thermally induced grating. Methods other than thermal should also be considered and tested experimentally including materials such as organic crystals, quantum well structures, and sol gels which can possess high third order nonlinear susceptibilities.

Actual experimental implementation of the switching and control elements described in this report is also recommended for further work. Whether the ultimate goal is an all-optical digital computer, optical processor, or optical communication system, certain logic and control functions must be implemented. As discussed in Section 3.4, OR, XOR, limiting, inversion and amplification should be readily achievable using

the phase grating approach. The good agreement between the experimental data and the thermal model, plus the ease with which the AND-gate was implemented instills confidence in the ability to successfully implement these additional functions. That these optical control functions were not demonstrated in this program was primarily due to the time limitations and limitations in the power output and spectral purity of the laser source. During the latter stages of the program, an ERIM-funded injection-seeded Q-switched frequency-doubled Nd:YAG laser was ordered from Quantel. Due to significant fabrication delays, the laser was not delivered until after the completion of the program. The injection-seeded Nd:YAG laser possesses transform-limited spectral purity, and high powers are available if needed, making it an ideal source for such experiments and should be used for any extensions of the work of this program.

Thermo-optical two-wave *mixing* for achieving amplification by coupling the energy from the stronger of two crossing beams of radiation into the energy of the weaker beam should also be pursued with the injection seeded Nd:YAG laser. Although efficient beam coupling or two-wave mixing has been demonstrated in photorefractive crystals [32], the time response is slow, on the order of a fraction of a second. Thermo-optic two-wave mixing, as discussed in Section 3.4.4.2, offers speeds on the order of a nanosecond and may be of particular value for optical implementations of associative memory or optical architectures employing iterative feedback loops.

The last area for further study is the implementation of multiple parallel channels. The AND-gate which was experimentally demonstrated in this program was a single element device. Since the real potential for optics lies in the parallelism of its operations, the experimental demonstration of a 2-D array is important. The single AND-gate structure appears to be well suited for extension to a 2-D array as discussed in Section 3.5. Such a 2-D structure should be implemented in

the laboratory and characterized for speed, efficiency, power and cross-talk.

The application of optical control concepts considered in this program is potentially quite extensive. The recommendations noted above are of course component oriented. It is also recommended that system oriented applications be pursued as a logical extension to the component development. Examples include switches, nonlinear operators, amplification and beam positioning for neural network optical computing, agile beam steering for sensor systems, and more generally, use in a wide range of analog or digital optical processing systems and in optical control devices.

Appendix A
THE THERMO-OPTIC COEFFICIENT FOR FLUIDS

The refractive index of a medium depends upon temperature, T, and density, ρ

$$n = n(T,\rho) \quad .$$

such that

$$dn = \left(\frac{\partial n}{\partial T}\right)_{\rho} dT + \left(\frac{\partial n}{\partial \rho}\right)_{T} d\rho \quad .$$

The density in turn depends upon temperature, T, and pressure, p

$$\rho = \rho(T,p)$$

such that

$$dn = \left[\left(\frac{\partial n}{\partial T}\right)_{\rho} + \left(\frac{\partial n}{\partial \rho}\right)_{T}\left(\frac{\partial \rho}{\partial T}\right)_{p}\right] dT + \left[\left(\frac{\partial n}{\partial \rho}\right)_{T}\left(\frac{\partial \rho}{\partial p}\right)_{T}\right] dp \quad .$$

In our experiments the refractive index grating is produced after pressure equilibrates such that the thermo-optic coefficient, dn/dT, at constant pressure is of interest

$$\left(\frac{dn}{dT}\right)_{p} = \left(\frac{\partial n}{\partial T}\right)_{\rho} + \left(\frac{\partial n}{\partial \rho}\right)_{T}\left(\frac{\partial \rho}{\partial T}\right)_{p} \quad .$$

This equation may be further simplified since the first term is usually much smaller than the second such that

$$\left(\frac{dn}{dT}\right)_{p} \doteq \left(\frac{\partial n}{\partial \rho}\right)_{T}\left(\frac{\partial \rho}{\partial T}\right)_{p} \quad . \qquad (A.1)$$

Since density, ρ, and volume, V, are inversely related by the mass, m

$$\rho = m/V$$

we have

$$\frac{1}{V}\frac{dV}{dT} = -\frac{1}{\rho}\frac{d\rho}{dT} \qquad (A.2)$$

Gases

The refractive index of a material medium is related to the amount of matter affecting the beam propagation. The refractive index of a vacuum is of course 1.0. For a gas, the increase in refractive index as matter is added to the vacuum can be described with good accuracy through the Dale-Gladstone relation [27]

$$(n - 1) = K\rho \qquad (A.3)$$

where ρ is the gas density and the proportionality constant K depends upon the polarizability or susceptibility of the molecules of gas. The density can be modeled to first order using the ideal gas law

$$pV = NkT$$

where N is the number of molecules in volume V and k is the Boltzmann constant. Therefore, using Eq. (A.2)

$$\frac{1}{\rho}\left(\frac{\partial\rho}{\partial T}\right)_p = -\frac{1}{T} \qquad (A.4)$$

Differentiating Eq. (A.3) and substituting along with Eq. (A.4) into Eq. (A.1), we have

$$\left(\frac{dn}{dT}\right)_p = \left(\frac{n-1}{\rho}\right)\left(-\frac{\rho}{T}\right) = -\left(\frac{n-1}{T}\right)$$

The thermo-optic coefficient for an ideal gas is therefore inversely porportional to temperature.

Liquids

For high density gases and liquids, the refractive index and density are more accurately related by the Lorentz-Lorentz law [27,28] (cf. the Claussius-Mossotti law [29])

$$\left(\frac{n^2 - 1}{n^2 + 2}\right) = K'\rho \tag{A.5}$$

where again the proportionality constant, here K', is determined by the nature of the material medium. Differentiating, we have

$$\frac{d\rho}{dn} = \frac{1}{K'}\left[\frac{2n}{n^2 + 2} - \frac{(n^2 - 1)2n}{(n^2 + 2)^2}\right]$$

$$= \frac{1}{K'}\frac{6n}{(n^2 + 2)^2} .$$

Using (A.5) we can eliminate the K' to obtain

$$\frac{dn}{d\rho} = \frac{(n^2 - 1)(n^2 + 2)}{6n\rho} \tag{A.6}$$

Substituting Eq. (A.6) into Eq. (A.1) and using Eq. (A.2), we have for the thermo-optic coefficient for fluids

$$\frac{dn}{dT} = -\frac{(n^2 - 1)(n^2 + 2)}{6n}\beta_v \tag{A.7}$$

where β_v is the volume coefficient of thermal expansion

$$\beta_v = \frac{1}{V}\frac{dV}{dT} = -\frac{1}{\rho}\frac{d\rho}{dT} .$$

Using tabulated values of β_v [30], the computed values of dn/dT are in good agreement with measured values of dn/dT [31]. This is particularly valuable since β_v is readily available for many liquids but dn/dT is more difficult to find.

We note in closing that although the relation in Equation (A.6) is quite accurate for liquids, it remains to be determined how accurate it is for plastics, glasses or crystals where the accuracy of Eq. (A.5) may be questionable and where the smallness of $(\partial n/\partial T)_\rho$ assumed in Eq. (A.1) may not be valid.

Appendix B
THERMAL DIFFUSION

Transient heat conduction or thermal diffusion is described by [19]

$$\frac{dT}{dt} = D\nabla^2 T \tag{B.1}$$

where T is the deviation of the temperature from its equilibrium value. The thermal diffusivity of the material medium is

$$D = \frac{\kappa_T}{\rho C_p} \tag{B.2}$$

where κ_T is the thermal conductivity, ρ is the mass density and C_p is the specific heat at constant pressure.

Thermal Grating Diffusion

For a thermal phase grating, T is a sinusoidal function which can be expressed as

$$T(x, t) = \Delta T(t) \cos Kx \tag{B.3}$$

where ΔT is the temperature half-amplitude and K is a spatial frequency

$$K = \frac{2\pi}{\Lambda} ,$$

Λ being the spatial wavelength of the sinusoid. Applying the ∇^2 operator we have

$$\nabla^2 T = -K^2 \Delta T \cos Kx \tag{B.4}$$

Equation (B.1) may therefore be rewritten as

$$\frac{dT}{dt} = -DK^2T \ .$$

Integrating, we obtain

$$\int_{\Delta T_o}^{\Delta T} \frac{dT'}{T'} = -DK^2 \int_0^t dt'$$

$$\ln \Delta T - \ln \Delta T_o = -DK^2t$$

$$\ln \frac{\Delta T}{(\Delta T)_o} = -DK^2t$$

$$\Delta T = (\Delta T)_o \, e^{-DK^2t} \qquad (B.5)$$

using Eq. (B.3). The amplitude of the stationary thermal wave can be seen to decay exponentially with a time constant of

$$t_d = \frac{1}{DK^2}$$

$$= \left(\frac{1}{2\pi}\right)^2 \frac{\Lambda^2}{D} . \qquad (B.6)$$

We may use Table II in conjunction with Eqs. (B.2) and (B.4) to calculate the thermal decay time. Using the physical parameters provided in Table II, the thermal diffusivity for liquid media is calculated to be on the order of 10^{-3} cm^2 sec^{-1}. For counter-

propagating beams where $\theta = 180^{o}$ (see Figure 3.1), Λ is a minimum (and so is t_d), equal to $\lambda/2$. The thermal decay time in a liquid for such a grating is approximately 2.5 nsec and is typical for STRS. For small angle (~0.1 rad) diffraction where Λ is about 10 λ, decay times are approximately 5 μsec and correspond to thermal diffusion in forced Rayleigh scattering (FRS) as shown in Table III.

Rayleigh Linewidth

It is interesting to note that the reciprocal of the lifetime of the thermal grating is equal to the half-width for Rayleigh scattering. The full linewidth (full-width at half height) is

$$\Gamma_R = \frac{2}{t_d} = 2DK^2 \tag{B.7}$$

where Γ_R has frequency units of radians per second. Expressed in units of Hz we have

$$\tilde{\Gamma}_R = \frac{1}{\pi t_d} = \frac{DK^2}{\pi}$$

The validity of Eq. (B.7) can be seen by taking the Fourier transform of the temporal exponential decay in Eq. (B.5)

$$\mathcal{F}\left\{e^{-t/t_d}\right\} = \frac{1}{\frac{1}{t_d} + i\omega}$$

$$= \frac{\frac{1}{t_d} - j\omega}{\left(\frac{1}{t_d}\right)^2 + \omega^2} \tag{B.8}$$

Such a bell-shaped frequency profile is referred to as a Lorentzian lineshape. The real part has a frequency half-width at

$$w = \frac{1}{t_d} = \frac{\Gamma_R}{2} \tag{B.9}$$

and the imaginary part is an "s-shaped" dispersion curve. For Rayleigh scattering of laser light, this Lorentzian profile is convolved with the laser line profile of full-width Γ_L to produce a scattered line profile of full-width

$$\Gamma = \Gamma_L + \Gamma_R.$$

Thermal Gaussian Diffusion

Instead of two interfering beams creating a thermal grating, if a single Gaussian shaped beam traverses an absorbing liquid a cylindrical volume is raised in temperature due to the absorption of radiation energy, and the temperature distribution in the traverse or radial direction is

$$T(x) = T(0)\, e^{-2x^2/w_o^2} \tag{B.10}$$

where w_o is the waist radius of the laser beam. It should be emphasized that T is not the temperature of the liquid but the temperature difference between the radiation-heated region and the surrounding liquid. Since the heated volume is cylindrically symmetric, and since the thermal distribution in the longitudinal or z-dimension is nearly constant, the ∇^2 operator in Eq. (B.1) becomes one-dimensional. Since the temperature distribution in the transverse or x direction seeks

equilibrium through diffusion as time increases, Eq. (B.1) may be rewritten as

$$\frac{\partial T(x,\ t)}{\partial t} = D\ \frac{\partial^2 T(x,\ t)}{\partial x^2}\ . \tag{B.11}$$

If we assume that the temperature distribution remains Gaussian as it diffuses then Eq. (B.10) may be rewritten as

$$T(x,\ t) = T(0,\ t)\ e^{-2x^2/w(t)^2} \tag{B.12}$$

and Eq. (B.11) becomes

$$\frac{dT(0,\ t)}{dt}\ e^{-2x^2/w(t)^2} = DT(0,\ t)\ e^{-2x^2/w(t)^2}\left[\left(\frac{4x}{w(t)^2}\right)^2 - \frac{4}{w(t)^2}\right] \tag{B.13}$$

Since we have assumed T to be a Gaussian function of x for all t, we need only to determine T as a function of t for x = 0. We may therefore rewrite Eq. (B.13) as

$$\frac{dT(0,t)}{dt} = D\ T(0,t)\left[-\frac{4}{w(t)^2}\right]\ . \tag{B.14}$$

If we assume the diffusion process to be adiabatic, then the energy contained in the thermalized region remains the same for all t. That is,

$$\int_{-\infty}^{\infty} T(0,t)e^{-2x^2/w(t)^2}\ dx = \int_{-\infty}^{\infty} T(0,0)e^{-2x^2/w_o^2}\ dx.$$

Solving these definite integrals [34] gives

$$T(0,t)\, w(t) = T(0,0)\, w_o$$

$$w(t) = w_o \frac{T(0,0)}{T(0,t)} .$$

Equation (B.14) may therefore be rewritten as

$$\frac{dT(0,t)}{dt} = DT(0,t) \left[- \frac{4}{w_o^2} \frac{T(0,t)^2}{T(0,0)^2} \right]$$

Separating variables and integrating

$$\int_{T(0,0)}^{T(0,t)} \frac{dT(0,t)}{T^2(0,t)} = \frac{-4D}{w_o^2\, T(0,0)^2} \int_0^t dt$$

$$\frac{1}{T(0,t)^2} - \frac{1}{T(0,0)^2} = \frac{8Dt}{w_o^2\, T(0,0)^2}$$

Rearranging and solving for $T(0,t)$ provides

$$T(0,t) = T(0,0) \left[\frac{8Dt}{w_o^2} + 1 \right]^{-1/2} .$$

If we call t_d the time it takes T to fall to one-half of its initial value due to diffusion, then

$$t_d = \frac{3\, w_o^2}{8D} \qquad (B.15)$$

Comparing Eq. (B.15) and (B.6) we see that the characteristic diffusion time is proportional to the square of the important transverse dimension of the temperature distribution and inversely proportional to the diffusion constant. A more equal comparison might compare the time required for T to fall to 1/e of its initial value as was done for Eq. (B.6). In this case Eq. (B.15) becomes

$$t_d^e = \left(\frac{e^2 - 1}{8}\right) \frac{w_o^2}{D} = 0.80 \frac{w_o^2}{D} , \tag{B.16}$$

more than twice as long as in Eq. (B.15).

Appendix C
TIME HISTORY FOR THERMO-OPTIC DISTURBANCES

In this appendix we look at the phenomenology associated with the passage of the laser pulse through an absorbing medium, and the transfer of radiation energy to that of the medium. We wish to look at the various transfer mechanisms in chronology and make estimates of the times involved in these transfer and relaxation mechanisms which ultimately lead to changes in refractive index and eventually to the decay or relaxation of the refractive index disturbance.

Absorption of the laser radiation by a liquid medium to which a dye has been added follows Beer's law and leads to an exponential decrease of the light intensity

$$I(z) = I(0)e^{-\alpha z}$$

where α is the absorption coefficient, z is the distance of propagation into the absorbing medium, and I(0) and I(z) are the light intensities at the entrance to the sample and at position z, respectively. At any particular position z_o, the amount of energy absorbed from the beam is

$$\int_0^t I(z,t)dt = \int_0^t I(0,t)e^{-\alpha z}dt$$

where I(0,t) is the temporal shape of the incident laser pulse.

The radiation energy absorbed leads to electronic excitation of the dye molecules in the liquid. These excited dye molecules undergo radiationless transitions back down to the ground state due to collisions with the solvent molecules. The energy of excitation is transferred to kinetic energy for the solvent molecules and occurs in a time on the order of 10^{-10} sec [14] for liquids [20]; see Table II.

The increased kinetic energy of the liquid molecules is manifest as an increased temperature in the spatial region of excitation. For these rapid thermalization times, the liquid volume or mass density does not have time to respond and so, along with the temperature increase, there is a pressure increase also. The laser beam has produced a bell-shaped cylindrical region of disequilibrium in both temperature and pressure.

Since there is no rigid confinement of the liquid, the increased pressure due to the laser heating is quickly dissipated. The rate at which the volume expands to relieve the local pressure increase is proportional to the acoustic velocity in the liquid divided by the size of the region of high pressure. In liquids, the velocity of sound is about 1 Km/sec (see Table II) and our volume of interest is about 30μm in diameter. The time for the pressure disturbance to go to equilibrium is therefore approximately 15 nsec. This represents the time in which the cylindrical volume excited by the laser expands due to the increased pressure. It therefore represents the time in which the liquid density increases or the time it takes for the refractive index guide to be created. This is roughly in quantitative agreement with the measured 20nsec time response for the onset of beam guiding as discussed in conjunction with Figure 2.3.

For our experiments involving two interfering beams in the focal region, the total diameter is again 30μm but interference fringes are produced such that a temperature and pressure grating are produced with a grating spacing of about 3μm. The pressure relaxation should take approximately 1.5 nsec and therefore about 1.5 nsec time delay before the refractive index grating is produced. This is in quantitative agreement with Figure 3.2 where we observe a 2 nsec delay between the passage of the exciting laser pulse and the onset of diffraction of our probe radiation.

It is interesting to note that if the two interfering beams are slightly different in wavelength, the interference fringes are moving. If this difference frequency is much larger than the reciprocal of this delay time then the fringes are washed out and no phase grating is generated. This places a coherence requirement upon the two beams and requires that the two beams be aligned to within a coherence length for the radiation. Also, if the frequency mismatch is equal to the reciprocal of the delay time for phase grating formation, then both the optical interference fringes and the density or phase grating move together at the same velocity in a direction perpendicular to the fringes, but the density grating lags behind the optical fringes by one half the grating spacing Λ, i.e. it is retarded by 90^{o}. This should allow coupling of one beam to the other via two wave mixing [30] especially if one beam is much stronger.

Once the pressure has come to equilibrium and is constant throughout the liquid, the temperature and density (or refractive index) profiles are bell-shaped (Gaussian) and match each other, except for the fact that the temperature is highest at the center and the density and refractive index are lowest at the center. These bell-shaped profiles widen and decrease at their central peak value as thermal diffusion leads to equilibrium (Appendix B). For the thermally generated beam guiding experiments where the transverse dimension is about 30μm, the diffusion time is about a millisecond. This is in quantitative agreement with our experimental observations as shown in Figure 2.3. For the thermal phase grating experiments where the important transverse dimension is not the beam width but the grating spacing, Λ (3μm in our experiments), the diffusion time is expected to be about 2 μsec. (See Table III.)

Appendix D
FIBER OPTICS

Since the beam guiding which we have observed experimentally during the course of this program is analogous to the creation of a real-time optical fiber, this appendix is used to provide some of the expressions which are useful in the study of optical fibers. It should be kept in mind that the thermally induced refractive index beam guide which we observed (1) does not have a constant diameter but decreases slowly as the radiation is focused to a waist, then increases slowly beyond the focus following a hyperbolic "ray-path", (2) the probing beam is similarly focused to a waist, and its dimensions are closely matched to the guide dimensions, (3) the graded index is a Gaussian function in the transverse dimension and, most importantly, (4) the sign of the Gaussian distribution is such that the refractive index in the guide region appears (based *upon* *thermal* analysis and interferometric measurements as discussed in Section 2.2.3) to be lower than in the surrounding liquid. This later attribute of our beam guide is particularly troublesome in explaining the observed guiding behavior but does appear to be compatible if we assume that the guiding action is the leaky wave type. None-the-less we assemble below some of the standard fiber optical properties keeping in mind the above caveats.

Mode Number

The numerical aperture for a fiber is equal to the sine of the acceptance half-angle, θ_a, for that fiber,

$$N.A. = \sin \theta_a$$

For a fiber immersed in a medium of refractive index n_o

$$N.A. = \frac{\sqrt{n_1^2 - n_2^2}}{n_o}$$

$$\doteq \frac{\sqrt{2n_1\Delta n}}{n_o}$$

where n is the maximum refractive index of the core, n_2 is the refractive index of the cladding, and $\Delta n = n_1 - n_2$ (n_1 is assumed greater than n_2).

The V-number normalized frequency, or normalized distance for a fiber is [23,24]

$$V = kr\sqrt{n_1^2 - n_2^2}$$

$$\doteq \frac{2\pi}{\lambda_o} r \sqrt{2n_1\Delta n} \qquad (D.1)$$

The number of modes which can be supported by a fiber is

$$N = \xi V^2 \qquad (D.2)$$

where $\xi = 1/2$ for a step index fiber, $\xi = 1/4$ for a quadratic graded index fiber, and ξ has comparable values for other forms of graded fibers.

Combining (D.1) and (D.2) shows that the number of modes which can be supported by a fiber is proportional to the square of its radius and proportional to the maximum refractive index difference between the core and cladding.

Reflection Coefficient

The amplitude reflection coefficient for an s-polarized or TE wave at a refractive index boundary is

$$r_s = -\frac{\sin(\theta_1 - \theta_2)}{\sin(\theta_1 + \theta_2)}$$

$$= \frac{n_1 \cos\theta_1 - n_2 \cos\theta_2}{n_1 \cos\theta_1 + n_2 \cos\theta_2}$$

$$= \frac{1 - \xi}{1 + \xi}$$

where the subscripts 1 and 2 refer to the incident and transmitted media, respectively, as shown in Figure D.1, and

$$\xi = \sqrt{1 + \frac{2n_1\Delta n + \Delta n^2}{n_1^2 \cos^2\theta_1}}$$

$$\Delta n = n_2 - n_1.$$

Optical waveguiding usually involves $\Delta n \ll n_1$ and θ_1 approaching 90°(i.e. grazing incidence). Similar equations for the TM or p-polarization are

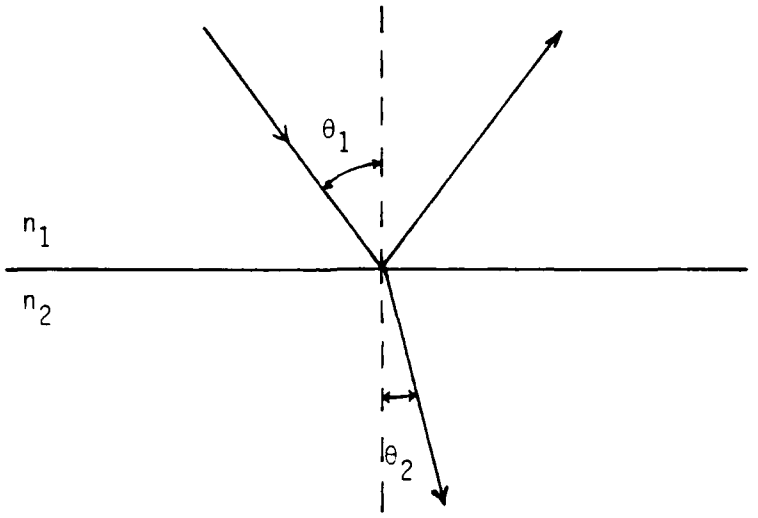

Fig. D.1 Reflection and refraction at a refractive index interface

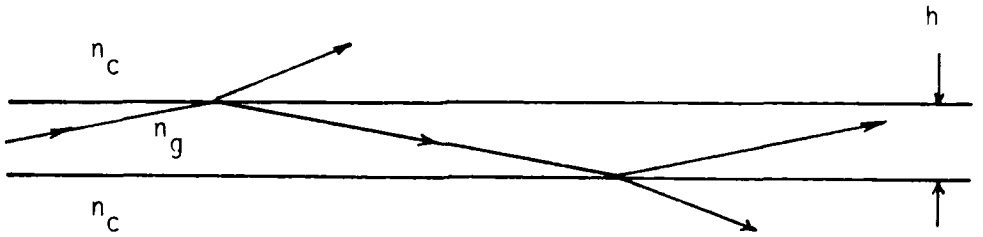

Fig. D.2 Leaky wave beam guiding. The guide index, n_g, is assumed to be less than the cover or cladding index, n_c.

$$r_p = \frac{\tan(\theta_1 - \theta_2)}{\tan(\theta_1 + \theta_2)}$$

$$= \frac{n_2 \cos\theta_1 - n_1 \cos\theta_2}{n_2 \cos\theta_1 + n_1 \cos\theta_2}$$

$$= \frac{\left(1 + \frac{\Delta n}{n_1}\right)^2 - \xi}{\left(1 + \frac{\Delta n}{n_1}\right)^2 + \xi}$$

Note that the negativity of r represents a 180° phase change upon reflection.

Rearranging terms, we can solve for ξ in terms of r

$$\xi = \left(\frac{1 - r_s}{1 + r_s}\right)$$

or

$$\xi = \left(1 + \frac{\Delta n}{n_1}\right)^2 \left(\frac{1 - r_p}{1 + r_p}\right) .$$

Assuming a high reflectivity of $r_s = 0.9$ ($r_s^2 = 81\%$) and n = 1.5, a Δn of 10^{-3} requires a grazing angle of $90° - \theta_1 = 0.66°$ or for a Δn of 10^{-4}, $90° - \theta_1 = 0.21°$. For $90° - \theta_1 = 4°$ and n = 1.5, a Δn of 10^{-3} leads to $r_s^2 = .037\%$ ($\xi = 1.129$).

Leaky Guiding

If one considers a slab waveguide whose thickness is h, which is clad on both sides by material whose refractive index is lower, then waveguiding can occur in the slab for radiation modes which are confined by total internal reflection (TIR) at the interface. If the cladding material has a higher index of refraction than the slab, then some radiation in the slab is partially transmitted by the interface and is lost from the slab. However, since the radiation is at near grazing angles, the amount reflected can be quite high resulting in only a small amount of radiation leaving the slab. The radiation propagates down the slab and is guided by it with the lost radiation serving as an attenuation factor. This is referred to as a leaky guide. A slab waveguide of thickness h, and refractive indices of the guide, n_g, and cladding, n_c, as shown in Figure D.2, has an exponential loss coefficient [24]

$$\alpha = \frac{\lambda_o^2}{8\sqrt{n_c^3 \Delta n}\ h^3}$$

where $\Delta n = n_c - n_g$. In a symmetric slab leaky guide, radiation is lost at the upper and lower interfaces. In a rectangular leaky guide, or a leaky fiber, radiation can be lost in the other two directions also so that α must be doubled. The transmission of a leaky fiber of length L is therefore

$$T = e^{-2\alpha L}$$

Choosing parameters analogous to our real-time beam guiding experiments of $h = 2w_o = 30\ \mu m$, $\Delta n = 10^{-3}$, $n_c = 1.5$, $\lambda_o = 0.51\mu m$, one computes $\alpha = 0.2\ cm^{-1}$. For a guide length of 1 mm, T is 98%. The efficiency of a

step index leaky fiber is computed to be high, and the guiding efficiency observed in our thermally induced beam guide experiments is also high.

It is worth noting that α depends on the third power of the guide thickness h. For our example above however, if h was halved, α would increase by 8-fold. However, T would only drop to 85 percent.

Appendix E
OPTIMIZING THE ABSORPTION COEFFICIENT

In the Appendix of the first semi-annual report for this program [10], we discussed the optimization of the absorption coefficient to maximize the gain for an injected signal in stimulated thermal Rayleigh scattering (STRS). We saw that the best choice of α, the absorption coefficient, is predicted to be equal to the reciprocal of the length of the sample in the direction of propagation. In this section we wish to make similar arguments to show that for STRS in generator experiments or for forced Rayleigh scattering, the best choice of α has a value equal to the reciprocal of the length from the entrance window of the sample to the focal region of focused radiation.

Equation (4.5) shows that the refractive index change, Δn, in the focal volume located a distance z_f from the entrance face of the sample depends upon α in a non-monotonic way. Qualitatively, a large value of α is desired for efficient conversion of laser radiation to thermal energy but too high a value of α leads to attenuation of the laser energy before it can work effectively in the focal volume. This is shown quantitatively by combining Eqs. (3.2) and (3.3) keeping only the functional dependence upon α

$$\Delta n(r) = \kappa(r)\alpha\, e^{-\alpha z_f}$$

where $\kappa(r)$ is a proportionality factor which depends upon the transverse dimension r. To find the best choice for α where Δn is a peak value, we differentiate Δn with respect to α and equate to zero,

$$\frac{d(\Delta n)}{d\alpha} = \kappa(r)\, e^{-\hat{\alpha} z_f} + \kappa(r)\alpha\, e^{-\hat{\alpha} z_f}(-z_f) = 0$$

or

$$1 - \hat{\alpha} z_f = 0.$$

We see that $\hat{\alpha}$, the optimum choice for α, is equal to the reciprocal of the distance of the focus

$$\hat{\alpha} = \frac{1}{z_f}$$

Further examination of the dependence of Δn upon α shows that a variation of α of $\pm$ 30 percent about $\hat{\alpha}$ results in Δn dropping by less than 10 percent.

REFERENCES

1. L.J. Cutrona et al., Proc. IEEE, Vol. 54, p. 1026, 1966.

2. I. Cindrich, J. Marks, A. Klooster, Proc. SPIE, Vol. 128, p. 128, 1977.

3. I. Cindrich, A. Tai, J. Fienup, anhd C. Aleksoff, Proc. SPIE, Vol. 185, p. 1, 1979.

4. H.J. Caulfield et al., Opt. Comm. Vol. 40, p. 86, 1981.

5. H.T. Kung and C.E. Leiserson, Proc. Symp. Sparse Matrix Computations and Their Applications, p. 9256, 1978.

6. See for example HM Gibbs, Optical Bistability: Controlling Light with Light. Academic Press, 1985.

7. L.M. Peterson, "Optical Control Using Stimulated Light Scattering," Opt. Eng. 25 (1986) 103; "Optical Switching Using Stimulated Rayleigh Scattering," SPIE 625 (1986) 87.

8. L.M. Peterson, Thermo-optical Beam Guide and Switching Experiments, Proc. of Topical Meeting on Optical Computing (OSA), Lake Tahoe, March 1987, pp. 217-220.

9. R.M. Herman and M.A. Gray, Phys. Rev. Lett. 19(15), 824 (1967); D.H. Rank, C.W. Cho, N.D. Foltz, and T.A. Wiggins, Phys. Rev. Lett. 19(15), 828 (1967); I. Batra, R. Enns, and D. Pohl, Phys. Status Solidi (B) 48, 11 (1971); and W. Kaiser and M. Maier, in Laser Handbook, F.T. Arecchi and E.O. Schulz-DuBouise, eds., North-Holland Publ. Co., New York (1972).

10. L. Peterson, "Optical Switching by Stimulated Thermal Rayleigh Scattering," ERIM Report No. 175900-8-T, June 1986, Ann Arbor.

11. D.W. Pohl, "Forced Rayleigh Scattering," IBM J. Res. Dev. 23 (5) (1979), 604; see special issue on dynamic gratings and 4-wave mixing, IEEE J. of Quant. Electr. QE-22 (8), pp. 1194-1542 (1986).

12. H.J. Eichler, P. Gunter and D.W. Pohl, Laser Induced Dynamic Gratings, Springer Verlag, 1986.

13. L. Peterson, "All-Optical Beam Control by Forced Rayleigh Scattering," ERIM Report No. 175900-11-T, December 1986, Ann Arbor.

14. K.F. Herzfeld and T.A. Litovitz, Absorption and Dispersion of Ultrasonic Waves, Academic Press, New York (1959).

15. M.G. Littman, H.J. Metcalf, "Spectrally Narrow Pulsed Dye Laser without Beam Expander", Appl. Opt. 17 (1978) 2224; "Single Mode Operation of Grazing Incidence Pulsed Dye Laser", Opt. Lett. 3 (1978) 138; "Single Mode Pulsed Tunable Dye Laser", Appl. Opt. 23 (1984).

16. AIP Handbook, D.E. Gray, editor, 2nd edition, McGraw-Hill, (1963).

17. P.A. Fluery and R.Y. Chiao, J. Acoust. Soc. Amer. 39, 751 (1966).

18. Y.R. Shen The Principles of Nonlinear Optics, Wiley Interscience, 1984.

19. Ibid, AIP Handbook, p. 4-77.

20. This is roughly 1000 times the mean free time between collisions for a liquid; $\tau_c \sim 10^{-13}$ sec, [14] Table 95-3.

21. R. Collier, C. Burchhardt, L. Lin, Optical Holography, Academic Press, 1971.

22. Optical Phase Conjugation, R.A. Fisher, editor, Academic Press (1983).

23. D. Marcuse, Light Transmission Optics, Van Nostrand, 1982.

24. Integrated Optics, T. Tamir, editor, Second Edition, Springer Verlag, 1982.

25. R.S. Longhurst, Geometrical and Physical Optics, Second Edition, John Wiley and Sons, New York, 1967.

26. J. Reitz and F. Milford, Foundations of Electromagnetic Theory, Addison-Wesley, 1960.

27. J.A. Stratton, Electromagnetic Theory, McGraw-Hill, New York, 1941.

28. Ibid, AIP Handbook, pp. 4-75.

29. Ibid, pp. 6-90.

30. See for example D. Staebler and J. Amodei, "Coupled Wave Analysis of Holographic Storage in $LiNbO_3$," J. Appl. Phys. 43 (1972) 1042 and J. Huignard and A. Marrachi, "Coherent Beam Amplification in Two-Wave Mixing Experiments with Photorefractive BSO Crystals," Opt. Comm. 38 (1981) 249.

31. T.Y. Chang, "Fast Self-Induced Refractive Index Changes in Optical Media: A Survey," Opt. Eng. 20 (1981) 220.

32. Standard Mathematical Tables, S.M. Selby, editor, Chemical Rubber Co., 1965.

33. I.L. Fabelinskii, Molecular Scattering of Light, Plenum, 1968.